Meteoritics & Planetary Science 1-27 (2025) doi: 10.1111/maps.70060

The fall of the Haag (LL4-6) chondrite breccia—Just 8 years after the nearby fall Stubenberg (LL6)

Addi BISCHOFF 1, Markus PATZEK 1, Jean-Alix BARRAT^{2,3}, Stig BARTEL⁴, Jasper BERNDT⁵, Henner BUSEMANN (1)⁶, Tommaso DI ROCCO⁷, Mattias EK (1)⁶, Manuela A. FEHR⁶, Dieter HEINLEIN⁸, Daniela KRIETSCH [D⁶, Björn LEHNERT⁹, Colin MADEN [D⁶, Oscar MARCHHART¹⁰, Martin MARTSCHINI¹⁰, Silke MERCHEL¹⁰, Andreas PACK⁷, Andrea PATZER¹¹, Marie PICHOTTA⁹, Maximilian P. REITZE¹, Philippe SCHMITT-KOPPLIN¹², Maria SCHÖNBÄCHLER 66, Leon THANNHEISER 13, Iris WEBER 1, Alexander WIESER 10, and Karl WIMMER¹⁴

¹Institut für Planetologie, University of Münster, Münster, Germany ²Univ Brest, CNRS, Ifremer, IRD, LEMAR, Institut Universitaire Européen de la Mer (IUEM), Plouzané, France ³Institut Universitaire de France, Paris, France ⁴VKTA—Strahlenschutz, Analytik & Entsorgung Rossendorf e. V., Dresden, Germany ⁵Institut für Mineralogie, University of Münster, Münster, Germany ⁶Institute of Geochemistry and Petrology, ETH Zürich, Zurich, Switzerland ⁷Universität Göttingen, Geowissenschaftliches Zentrum, Göttingen, Germany ⁸German Fireball Network, Augsburg, Germany ⁹Technische Universität Dresden, Institut für Kern- und Teilchenphysik, Dresden, Germany ¹⁰Faculty of Physics, Isotope Physics, University of Vienna, Vienna, Austria ¹¹Natural History Museum Vienna, Vienna, Austria ¹²Helmholtz-Zentrum, München, German Research Center for Environmental Health, Analytical BioGeoChemistry, Neuherberg, Germany ¹³Prücknerstraße, Hof, Germany ¹⁴Salvatorgasse, Nördlingen, Germany

*Correspondence

Addi Bischoff, Institut für Planetologie, University of Münster, Wilhelm-Klemm-Str. 10, D-48149 Münster, Germany. Email: bischoa@uni-muenster.de

(Received 14 June 2025; revision accepted 22 September 2025)

Abstract—On October 24, 2024, an impressive fireball was visible over Austria. After the possible strewn field was calculated, the first sample of the Haag meteorite, with a mass of 8.76 g, was discovered on November 2, 2024, 8 days after the fireball event. Four more samples were found afterward putting the total sample mass at about 151 g. Short-lived radionuclides were measured shortly after recovery on a small sample, which was also used for almost all analyses presented here. Results confirm that the Haag meteorite derived from the bolide fireball event. Haag is a severely fragmented ordinary chondrite breccia and consists of typical equilibrated and recrystallized lithologies (LL4-6) as well as impact-related lithic clasts, such as dark, fine-grained impact breccias. Most fragments are highly recrystallized (type 6), but some show a well-preserved chondritic texture, which is of petrologic type 4 since the olivines are equilibrated. The olivines in the bulk rock have Fa contents of $29.5 \pm 0.5 \text{ mol}\%$, whereas the low-Ca pyroxenes have compositions of Fs_{23.9±1.4}Wo_{1.6±0.7} with slightly variable Fs contents up to 28 mol%. However, the occurrence of type 3 fragments in other parts of the rock cannot completely be ruled out. Many clasts are moderately shocked (S4; C-S4). Using the fragment with the lowest degree of shock to determine the bulk rock's shock degree, Haag has an overall shock degree of S2 (C-S2). The LL chondrite classification is also supported by O isotope data, A. Bischoff et al.

the results of bulk chemical analysis, and the physical properties of density and magnetic susceptibility. The nucleosynthetic Ti and Cr isotope data confirm that Haag is an ordinary chondrite, related to the noncarbonaceous (NC) meteorites. Haag does not contain detectable amounts of solar wind-implanted noble gases, and we rule out any substantial exposure at the direct surface of the parent body. Based on noble gases, Haag has an exposure age of 21–24 Ma and a pre-atmospheric meteoroid radius of 20–85 cm with a sample depth between 4 and 5 cm below the meteoroid surface, consistent with constraints from cosmogenic radionuclides. The soluble organic compositions of Haag are consistent with the profiles of the Stubenberg (LL6) breccia and show characteristics consistent with the complex shock, brecciation, and lithification history of the breccia. Haag and Stubenberg fell near each other (110 km away) within just 8 years. Since only 8.5% (about 110) of meteorite falls worldwide are LL chondrites, it is remarkable that two LL chondrites fell near each other in such a short time.

INTRODUCTION

A fireball with the brightness of a full moon was observed over the northeastern part of Austria on the evening of Thursday, October 24, 2024, at 21:24:38 local time (EN241024; Spurný & Borovička, 2025). Visual sightings from Austria, Czechia, Germany, and Slovakia were reported (https://fireballs.imo.net/members/imo_view/event/2024/6300). The bolide was registered by about 15 stations of the European Network (in Czechia, Slovakia, and Austria; Data from Pavel Spurný, Jiří Borovička, and Lukáš Shrbený: https://www.asu.cas.cz/~meteor/bolid/2024_10_24/), by several video camera stations of the Allsky7 Network and with dash cams.

During entry into the atmosphere (see Spurný and Borovička (2025) for details), the meteoroid lost a part of its original mass, and the remaining rock fragmented into many pieces, which fell (displaced by high-altitude winds) in a strewn field near the township of Haag, Lower Austria (Figure 1). Due to the rapid publication of these facts via the Internet, the news of the meteorite fall in Austria quickly spread and reached relevant forums. Soon, an eager search for the freshly fallen meteorites began. Five individual meteorite samples totaling a mass of \sim 151 g were recovered within an area of about 5 km \times 1.5 km (Figure 1).

On Saturday, November 2, 2024, one of the authors (LT) was the first to report the recovery of a stony meteorite weighing 8.76 g, mostly covered with a fresh fusion crust (sample H01; Table S1). He immediately brought this first discovery to Augsburg to another of this study's authors (DH) for examination and offered the material for scientific analysis. Subsequently, 2.79 g of this material was donated to the Institut für Planetologie (University of Münster, Germany) for analysis and classification, and the main remaining piece of 5.97 g was immediately transferred to Dresden (Germany) for gamma spectroscopy of the short-lived radionuclides. Further successful meteorite finds were reported in the following

days by two dedicated searchers from Poland. On November 3rd, a piece weighing 3.49 g was discovered (H02), and on November 6th, a larger meteorite piece of 46 g (dry: 45.38 g; H03; Table S1) was found. A family living within the strewn field found unusually shaped fragments one day after the fireball event on October 25, 2024. The stone (H04) apparently hit the roof of their house and then broke into fragments on their property's asphalt parking lot. These pieces were recognized as meteorites 2 months later, on December 29, 2024, and the stony meteorite fragments totaling 28.61 g (18.55 g, 9.21 g, 0.74 g, and 0.11 g crumbs) were secured. The main mass of the meteorite fall was not found until the winter vegetation on a field had disappeared in spring: On April 5, 2025, a meteorite individual weighing 64.06 g (H05; Table S1) with almost complete fusion crust was discovered by an Austrian searcher. Images of typical locations of the find area are given in Figure 1. The landscape largely consists of hilly farmland, which is mainly used to grow winter barley or winter rapeseed. Small sections of pine forest and rows of fruit trees often border the cultivation areas.

In this report, we present the mineralogical, physical, chemical, isotopic, and spectroscopic characteristics of the new meteorite, which include data on organics, short- and long-lived cosmogenic radionuclides, and magnetic susceptibility. The meteorite named "Haag" has been accepted by the Nomenclature Committee (The Meteoritical Bulletin, 2025). The coordinates are 48°07′33.6″ N and 14°35′00.2″ E. After the meteorite fall in Braunschweig in 2013 (L6; Bartoschewitz et al., 2017), Haag represents the 13th recovered meteorite fall within a relatively small area in Central Europe (see below). Fewer than 10 meteorite falls per year are recovered globally; hence, this concentration of recorded falls is remarkable.

SAMPLES AND METHODS—SUMMARY

Different analytical methods were performed to obtain information about the meteorite class of the

FIGURE 1. (a) Locations of the five meteorites found in the Haag strewn field with weights in grams. Source of base map: Google Earth. https://www.google.com/intl/de_in/earth/. (b, c) Typical location areas of the strewn field. (b) Hilly farmland, cultivation of winter barley in the suggested 20–30 g mass range find area, 500 m east of Haag-Schudutz. (c) Farmland and pear trees in the strewn field 500 m west of Oberndorf. (d) The first recovered sample (H01) of the 8.76 g fragment found November 2, 2024. (e) Cut piece of H01.

Haag sample and to reveal details on chemical, physical, isotopic, and mineralogical features and characteristics of the sample. In this section, the studied

samples and the analytical procedures are briefly summarized. More details are given in the Supporting Information.

on Wiley Online Library for rules of use; OA articles are governed by the applicable Creative Commons Licenso

A. Bischoff et al.

TABLE 1. Mean chemical composition of the main oxide phases in Haag.

	Olivine	Px	Ca-Px	Plag	Plag-An ₆₅	Apatite	Chromite
	n = 82	n = 28	n = 9	n = 7	n = 1	n = 4*	n=6
SiO ₂	36.8 ± 0.4	53.6 ± 0.9	51.7 ± 0.7	63.0 ± 1.3	48.3	0.17	0.07
TiO_2	0.13	0.16	0.42	0.08	0.07	0.13	2.35 ± 0.7
Al_2O_3	< 0.02	0.29	0.64 ± 0.3	20.8 ± 1.0	29.3	< 0.03	6.2 ± 0.4
Cr_2O_3	< 0.03	0.16	0.80 ± 0.2	< 0.03	1.46	< 0.02	57.2 ± 0.5
FeO	26.3 ± 0.4	15.5 ± 0.8	5.7 ± 1.0	0.65	1.22	0.71	31.5 ± 0.7
MnO	0.46	0.46	0.24	< 0.02	< 0.04	< 0.02	0.60
MgO	35.2 ± 0.5	27.2 ± 0.9	16.5 ± 0.9	0.35	0.57	0.08	1.39 ± 0.1
CaO	< 0.02	0.78 ± 0.36	20.6 ± 2.3	1.84 ± 0.4	13.1	52.0 ± 0.3	< 0.01
Na ₂ O	< 0.01	0.07	0.59 ± 0.2	10.2 ± 0.4	3.9	0.33	< 0.01
K_2O	< 0.01	< 0.01	< 0.02	0.41 ± 0.1	0.07	< 0.02	< 0.01
P_2O_5	< 0.04	< 0.02	< 0.02	< 0.03	< 0.01	40.1 ± 0.3	< 0.01
Total	99.04	98.25	97.23	97.41	98.04	100.21*	99.35
Fa	29.5 ± 0.5						
Fo	70.5 ± 0.5						
Fs		23.9 ± 1.4	9.3 ± 1.6				
Wo		1.6 ± 0.7	42.8 ± 4.5				
An				8.9 ± 2.0	64.9		
Or				2.4 ± 0.8	0.4		

Note: All data in wt%; n = number of analyses. Px = low-Ca pyroxene (Fs₂₀₋₂₈); Ca-Px = Ca pyroxene; $Plag = \text{typical plagioclase } (An_{6-11})$. * = contains 6.2 wt% Cl and 0.4 wt% F. The An₆₅-plagioclase analysis is contaminated by surrounding chromites.

Haag specimen H01 was cut and ~2.5 g was used for further studies. Two polished thin sections were prepared from H01 (PL24076, PL24077), as was one thick section (PL25009). The fusion crust was carefully removed from one broken piece of H01, and 0.59 g of the specimen was homogenized for chemical, isotopic, and spectroscopic studies. In addition, a polished thick section (No. O3806) from sample H04 was studied in Vienna (Austria), and the magnetic properties were obtained on the H02 and H05 specimens.

The two thin sections and the thick sections were used for optical and scanning electron microscopy (SEM) at the Institut für Planetologie (University of Münster) and at the Natural History Museum (NHM) in Vienna (Austria). Most chemical data were obtained by electron microprobe analysis (EPMA) at the Institut für Mineralogie (Münster) and presented in Tables 1 and 2 (see also the Supporting Information).

After preparing a homogenous powder of ~0.59 g from H01, a whole-rock sample of ~110 mg was analyzed for major and trace element concentrations by inductively coupled plasma sector field mass spectrometry (ICP-SFMS) at the University of Brest (France) following the procedure described by Barrat et al. (2012, 2016). Cosmogenic as well as primordial radionuclide concentrations were analyzed by nondestructive gamma spectrometry in the underground laboratories in Dresden (Germany) (Bemmerer et al., 2025; Niese et al., 1998). More details are given in the Supporting Information.

At the University of Göttingen, the bulk oxygen isotope composition was analyzed by means of laser fluorination in combination with gas source mass spectrometry. More information is presented in the Supporting Information and given in Pack and Herwartz (2014), Herwartz et al. (2014), Pack et al. (2016, 2017), and Peters et al. (2020).

For the Ti and Cr isotope analyses, a powdered sample of Haag (H01; 21.8 mg) was dissolved and purified using ion exchange chromatographic procedures. Titanium and Cr isotope analyses were carried out using a Thermo Fisher Scientific Neptune Plus multicollector inductively coupled plasma mass spectrometer (MC-ICPMS) at the Institute of Geochemistry and Petrology at ETH Zurich. The dissolution procedure follows Bischoff, Barrat, et al. (2019) and the Ti and Cr separation and measurement protocols are described in Rüfenacht et al. (2023) and Williams et al. (2021). The data are reported relative to an in-house Alfa Aesar Ti wire standard and the NIST SRM 979 Cr standard in the ε-notation applying the sample-standard bracketing method: ε^i Ti = $({}^i\text{Ti}/{}^{47}\text{Ti}_{\text{sample}})/({}^i\text{Ti}/{}^{47}\text{Ti}_{\text{standard}}) - 1)$ × 10^4); i = 46,48,50 and ε^i Cr = $({}^i\text{Cr}/{}^{52}\text{Cr}_{\text{sample}})/({}^i\text{Ti}/{}^{47}\text{Ti}_{\text{standard}}) - 1$ $({}^{i}Cr/{}^{52}Cr_{standard}) - 1) \times 10^{4}); i = 53,54.$

Both methods analyzing cosmogenic nuclides used powdered aliquots of the 0.59 g sample from H01. The noble gases He-Xe present in the bulk sample were analyzed at ETH Zurich using three aliquots of H01 (A, B, and C) and the standard procedures are described in

Kamacite Taenite Tetrataenite Troilite Element n = 9n = 25n = 27n = 10 50.1 ± 1.6 91.3 ± 1.4 60.2 ± 3.6 62.3 ± 1.0 Fe Co 4.3 ± 1.1 1.41 ± 0.42 0.94 ± 0.32 0.09 Ni 5.1 ± 0.9 38.4 ± 3.8 48.5 ± 1.7 < 0.02 S < 0.01 0.05 0.07 34.7 ± 0.7 Total 99.61 100.71 100.06 97.11

TABLE 2. Mean chemical composition of metals and sulfide (troilite) from the Haag breccia.

Note: All data in wt%.

detail by Riebe et al. (2017). See the Supporting Information for more details as well as Nier (1950), Steiger and Jäger (1977), Busemann et al. (2000), and Leya and Masarik (2009). Instrumental accelerator mass spectrometry (IAMS) was used to detect long-lived cosmogenic radionuclides ²⁶Al and ⁴¹Ca using the unique procedures developed at the Vienna Environmental Research Accelerator (VERA) (Martschini et al., 2022).

The meteorite's magnetic susceptibility (MS) was measured with the handheld device SM-30 from ZH (www.zhinstruments.cz) in Nördlingen (Germany) following CT scan techniques to obtain the correct density, and mid-infrared (IR) spectroscopic measurements were undertaken at the Institut für Planetologie (University of Münster, Germany). A destructive methanolic solvent extraction of organic matter was performed in an agate mortar using 5 mg of powder from the Haag meteorite at the Helmholtz-Zentrum, München (Germany). Analytical details and information on data processing are given in Schmitt-Kopplin et al. (2010, 2012), Tziotis et al. (2011), Hertkorn et al. (2015), and Ruf et al. (2017). More details about our methods can be found in the Supporting Information.

RESULTS

Petrography and Mineralogy

Description of Hand Specimens

About 90% of H01 was covered by a black fusion crust (Figure 1). In some areas, the crust was broken off and the grayish interior was visible, indicating a brecciated texture of the bulk rock. In some parts, minor soil residue from the impact location was still attached to the meteorite fragment. In addition, distinct features of once molten components were locally observed at the surface of H01 as well as H02 (Figure S1), probably related to former sulfide (Figure S1e) and metal components (Figure S1f) in the rock. The second find, H02, has a pyramidal shape (Figure S1) and computed tomography (CT) slices show some details of the interior of the sample (Figure S2). With a mass of 3.49 g and a volume of 1.094 cm³, it has a bulk density of

3.187 g/cm³. Its surface area of 5.58 cm², which shows several very fine cracks, consists of 73% black fusion crust with prominent flow lines and 22% smooth fusion crust of brownish color. The primary crust is missing on 5% of the surface area, revealing the gray interior of the stony meteorite, partially covered with a wafer-thin secondary fusion crust. The largest meteorite of the fall H05, which is almost completely covered with black fusion crust, has a volume of 20.05 cm³. It has a bulk density of 3.194 g/cm³ and a surface area of 44.41 cm², as obtained with a surface scanner (Figure 2).

Mineralogy and Petrography

Studying the thin sections prepared from H01, it is clearly visible that the rock is a complex chondritic breccia (Figure S3). Haag consists of highly equilibrated and recrystallized lithologies (types 5 and 6) as well as very few less equilibrated lithologies of type 4 (Figure 3). The boundaries between the various fragments are well defined, and the embedding material is a fine-grained clastic matrix (Figure 3d). Locally, abundant small pores are present in many minerals, especially in the feldspar-rich mesostasis areas of chondrules. Different types of chondrules, including barred olivine (BO), porphyritic olivine-pyroxene (POP), and porphyritic pyroxene chondrules (PP), are well preserved in type 4 fragments (Figure 4). In clasts of higher petrologic grade (types 5 and 6), they are barely recognizable and merge with the fragments' matrix due to metamorphic recrystallization. As in most ordinary chondrites, some Al-rich objects are present (e.g., Bischoff & Keil, 1983a, 1983b, 1984; Ebert & Bischoff, 2016a). One Al-rich chondrule is shown in Figure 4d and its bulk composition is rich in Na₂O (6.4 wt%; Table 3). It mainly consists of a Na, Al-rich mesostasis embedding olivine grains and skeletal low-Ca pyroxene laths (Figure 4d). The bulk composition is plagioclase normative and also has about 15.5 wt% Al₂O₃, 57.8 wt% SiO₂, and 3.4 wt% CaO (Table 3). A second Al-rich object is egg-shaped (perhaps a deformed chondrule) and has a similar composition (Figure 5e; Table 3).

Besides the typical chondritic clasts of types 4–6 (Figure 3a–c), some unusual fragments were recognized.

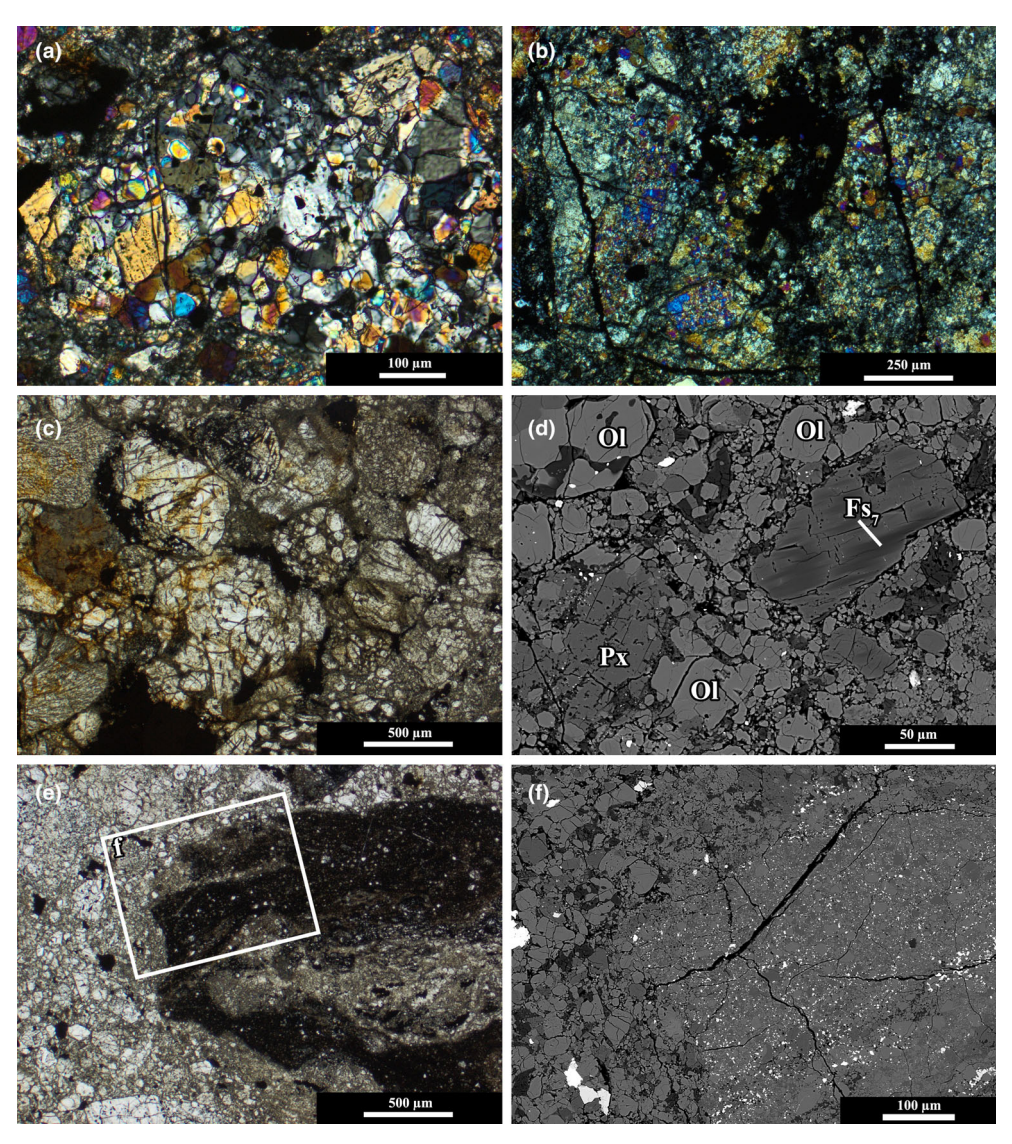


FIGURE 2. Different types of fragments in Haag. (a) Coarse-grained type 6 fragment; polarized light, crossed nicols. (b) Fine-grained type 6 fragment; polarized light, crossed nicols. (c) Type 4 fragment with well-defined chondrules; polarized light. (d) Typical view of the clastic matrix showing a clast with rare Fs-poor low-Ca pyroxene (\sim Fs₇); Ol = olivine, Px = low-Ca pyroxene; BSE image. (e) Dark impact-related fine-grained fragment; polarized light. (f) BSE image of details from the impact-related fine-grained fragment shown in (e); most of the small light grains are troilite.

One of these is a dark, impact-related clast having areas of abundant fine-grained distributed opaque minerals and an inhomogeneous texture. The central part is coarser grained and more transparent than the outer areas (Figure 3e,f). Chemically, the mean bulk composition of the clast is similar to that of the bulk meteorite, except for having significantly lower Ni and somewhat lower S concentrations (Table 3). Another unusual fragment is brownish in transmitted light (Figure 5b). The impact-related fragment is feldspar normative in composition (Al₂O₃: ~29 wt%; CaO: ~12 wt%; Na₂O: ~3 wt%; Table 3) and its groundmass could be bytownitic plagioclase as obtained by IR spectroscopy (Figure S4).

The fragment also contains abundant Cr_2O_3 (~5 wt%; Table 3). Thus, the composition may point toward a processed earlier Ca,Al-rich object that suffered metamorphic alteration, indicated by an exchange of Mg in spinel by Cr and Fe, as is often observed in thermally processed Al-rich objects from noncarbonaceous chondrites (Bischoff & Keil, 1983b, 1984; Rout et al., 2010).

Olivine and low-Ca pyroxene are by far the most abundant phases throughout all polished sections. The olivines are homogeneous in composition, and the mean composition of 82 randomly and automatically analyzed olivines (grid analysis) was found to be $Fa_{29.5\pm0.5}$ with a very limited compositional range between 28.0 and

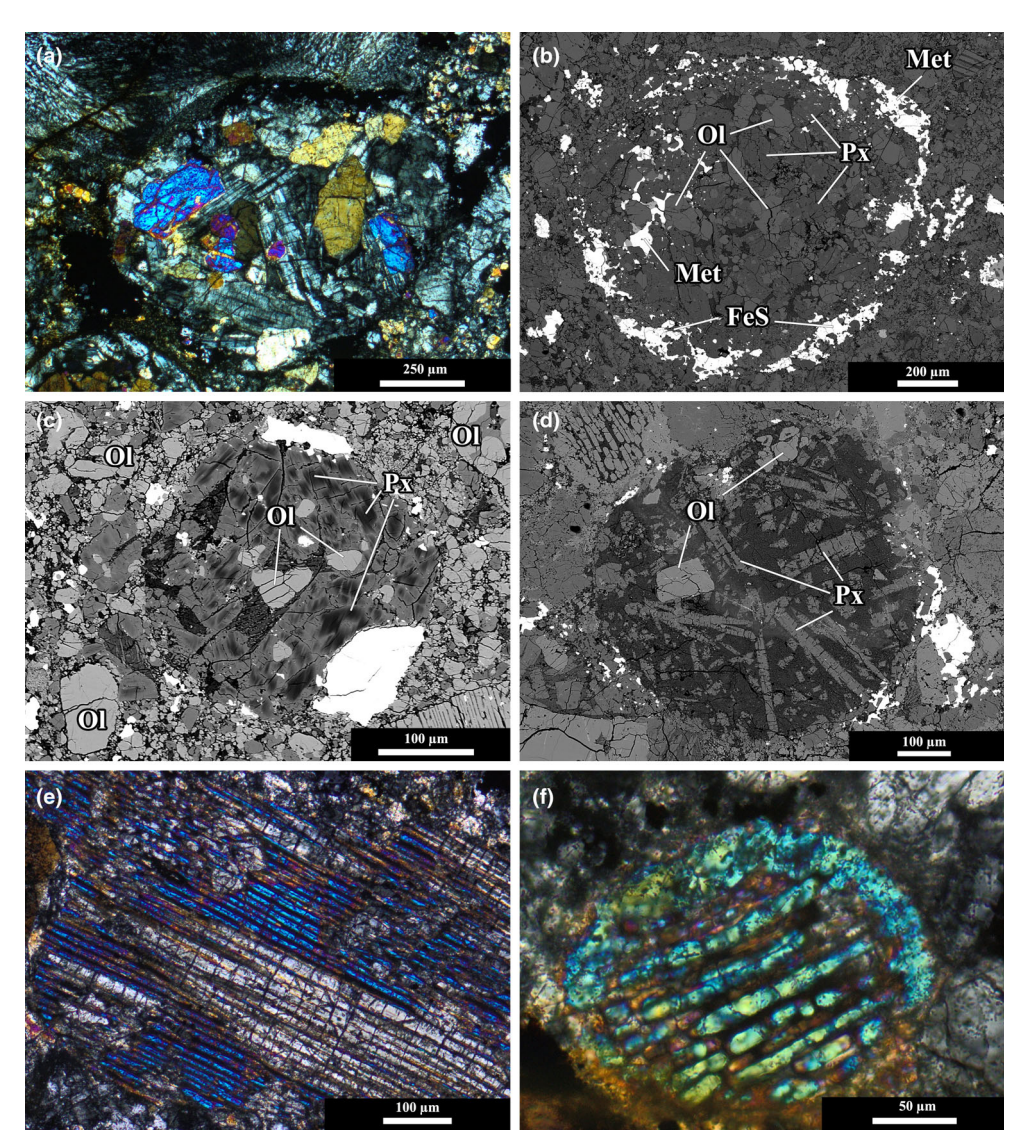


FIGURE 3. Chondrules in Haag. (a) Porphyritic olivine–pyroxene (POP) chondrule; polarized light, crossed nicols. (b) Some of the porphyritic chondrites have well-defined rims of abundant troilite; Ol = olivine, Px = low-Ca pyroxene, FeS = troilite, Met = metal; BSE image. (c) Porphyritic olivine–pyroxene (POP) chondrule with equilibrated olivine (Ol; Fa_{29.8}) and strongly zoned low-Ca pyroxenes (Fs_{5.7-22.7}); BSE image. (d) Al-rich chondrule (Table 3); olivine grains (Ol) and low-Ca pyroxene (Px) laths are embedded in a fine-grained Al-rich mesostasis; BSE image. (e) Part of a large (>1 mm) barred olivine (BO) chondrule; polarized light, crossed nicols. (f) Small barred olivine chondrule (BO); polarized light, crossed nicols.

31.1 mol% Fa (Table 1). This value is typical for equilibrated LL chondrites, and we found no unequilibrated olivines in all analyzed sections; however, we frequently noticed a TiO_2 concentration of up to 0.4 wt% in many grains, probably related to the occurrence of small Ti-bearing inclusions in many olivines. Randomly analyzed low-Ca pyroxenes have compositions of $Fs_{23.9\pm1.4}Wo_{1.6\pm0.7}$ (n=28; Table 1), and the Fs contents vary between 20 and 28 mol%. An individual search for unequilibrated components revealed a few Fe-poor low-Ca pyroxenes (down to \sim Fs₅) but no Fa-poor olivine. Especially in the thick section in Vienna

(No. O3806), fragments and chondrules (Figure 4c) with zoned low-Ca pyroxenes were frequently observed. The Ca pyroxenes have a mean composition of Fs_{9.3}Wo_{42.8} (Table 1), but the Fs and Wo contents vary from 9 to 13 mol% and 32 to 45 mol%, respectively.

By far, most plagioclase, which can be as large as 300 μ m in size (Figure 5a), is Ab-rich, and the analyses were mainly obtained from plagioclase within the recrystallized type 5 and type 6 fragments (compare Figure 3). The mean composition revealed a value of Ab_{88.7}An_{8.9}Or_{2.4} (Table 1) with a variable composition between 6 and 11 mol% An; however, Ca-rich

FIGURE 4. Details from the Haag chondrite. (a) Large, 300 μm plagioclase grain (~An₇; gray); polarized light, crossed nicols. (b) Brownish, unusual fragment; polarized light. Insert: Detailed BSE image showing small chromite grains in a Ca-plagioclase-normative (~An₇₅) groundmass. (c) Cu-grain (Cu) within a metal–sulfide (Met-Sulf) association; reflected light. (d) Assemblage of opaque phases with kamacite (Kam), taenite (Tae), troilite (Troi), and chromite (Chr); BSE image. (e) Egg-shaped plagioclase-normative object (Table 3) next to a recrystallized BO chondrule; BSE image. (f) Chromite (Chr)-rich vein rimmed by plagioclase (Plag) within an olivine-rich clast; Ol = olivine; BSE image.

plagicalse was also detected, having an An content of ~65 mol%.

Based on their size, chromites were also easily found and analyzed in the metamorphosed clasts. Chromites are relatively homogeneous in composition, with 57.2 wt% Cr₂O₃ and 31.5 wt% FeO (Table 1). In one case, an unusual chromite-rich vein rimmed by plagioclase was found within an olivine-rich clast (Figure 5f). Similar associations were earlier studied by Rubin (2003). So far, only one merrillite grain was detected. Apatite is rich in Cl (6.2 wt%; Table 1) and similar in composition to those reported from Ward et al. (2017) for many other ordinary

chondrites. A few ilmenites were detected as accessory mineral phases.

Sulfides (with areas up to 3 mm in length; Figure S2) were found to be abundant throughout all the thin sections, and their mean compositions are given in Table 2. The sulfide is pure troilite, with 34.7 wt% S and 62.3 wt% Fe (Table 2). Four different metals were observed: kamacite, taenite, tetrataenite, and native Cu (Figure 5c). The Ni and Co concentrations of kamacite do not show significant variations (mean: 5.1 wt% and 4.3 wt%, respectively). The mean taenite composition has an Ni content of 38.4 wt% and a Co content of ~1.4 wt

19455100, 0, Downle aded from https://onlinelibrary.wiley.com/doi/10.1111/maps.70060 by Helmholtz Zentrum Muenchen Deutsches Forschungszentrum, Wiley Online Library on [14/10/2025]. See the Terms and Conditions (https://onlinelibrary.wiley.com/term) on Wiley Online Library for rules of use; OA articles are governed by the applicable Creative Commons Licenso

TABLE 3. Chemical compositions of the unusual brownish clast, the dark impact clast (both microprobe analyses), and two Al-rich objects in Haag.

-	//	3	C	
	Brown, Cr-rich object (Figure 5b)	Large dark impact clast (Figure 3e)	Al-rich Chondrule (Figure 4d)*	Egg-shaped Al-rich object (Figure 5e)*
SiO ₂	41.7	41.2	57.8	53.8
TiO_2	0.23	0.24	0.65	0.51
Al_2O_3	29.4	2.78	15.5	11.5
Cr_2O_3	5.3	0.72	0.66	0.71
FeO	4.0	20.9	7.0	10.8
MnO	0.07	0.37	0.14	0.27
MgO	0.93	25.0	8.1	14.2
CaO	11.7	2.05	3.4	2.82
Na ₂ O	2.85	1.35	6.4	5.3
K_2O	0.04	0.10	0.20	0.11
P_2O_5	0.10	0.16	n.d.	n.d.
S	0.05	1.34	0.11	0.07
Ni	< 0.01	0.12	0.10	n.d.
Total	96.39	96.33	100.0	100.09

Note: All data in wt%; *EDS analysis normalized to 100%. Abbreviation: n.d., not detected.

%; however, we cannot rule out that this observation reflects the analyses of fine-grained intergrowths of taenite and kamacite. Several grains of tetrataenite (\sim Fe₅₀Ni₅₀) were also detected (Table 3). The metals reach a size of 1 mm in largest dimension (Figure S2).

Shock Metamorphism and Terrestrial Weathering

As stated above, based on the study of the thin sections, Haag is heavily brecciated (Figure 3). The shock degree varies from clast to clast. Within some clasts, plagioclase and olivine show undulatory extinction (S2; C-S2), whereas in most other fragments, olivines show distinct sets of planar fractures (S3 (C-S3); Figure 6a) or have been shock-mosaicized (S4 (C-S4); Figure 6b; Stöffler et al., 1991, 2018; Bischoff & Stöffler, 1992; Bischoff, Schleiting, & Patzek, 2019).

Among the great variety of clasts, one example is the dark impact-generated clast shown above (Figure 3e,f). In addition to this dark clast, we observed fragments with deformed chondrules (Figure 6c) or with shock-darkened areas (Figure 6d). Other fragments have thin shock veins (Figure 6e,f). The shock veins are restricted to individual lithic clasts and do not crosscut the bulk rock. In some cases, they also occur at the borders of the clastic matrix.

As expected for a fall, the weathering degree of Haag is W0. However, we observed local areas on the rock's surface already showing a brownish tinge, resulting from the first breakdown of metals. This represents a weathering effect during the rock's residence time of

about 8 days on the wet ground. In thin sections, minor rinds of alteration products (iron oxides-hydroxides) can be found surrounding metal grains.

Mid-Infrared (IR) Spectroscopy

To study the spectroscopic characteristics of the rock, a bulk sample powder was analyzed by mid-IR spectroscopy. Measurements were performed in the range between 7 µm and 14 µm, which is the region covered by the MERTIS instrument onboard the BepiColombo spacecraft (Hiesinger et al., 2020; Weber et al., 2018, 2023). The infrared spectrum of the investigated sample aliquot (Figure 7) shows a clear Christiansen feature (CF) at $8.70 \, \mu \text{m}$ (1149 cm⁻¹), which is, however, not the global minimum in the spectrum. Five Reststrahlen bands (RB) appear at 9.09 μm (1101 cm⁻¹), 9.55 μm $(1047 \text{ cm}^{-1}),$ 10.29 μm $(972 \text{ cm}^{-1}),$ 10.77 um (929 cm^{-1}) , and $11.26 \mu\text{m}$ (888 cm^{-1}) . A broad transparency feature (TF) is located between ~11.89 µm (841 cm^{-1}) and 13.87 µm (721 cm^{-1}) with a maximum at 12.53 μm (798 cm⁻¹).

Oxygen Isotopes

The O isotope compositions of a Haag aliquot (H01; 2.258 mg) were measured: $\delta^{17}O = 3.945 \pm 0.126\%$, $\delta^{18}O = 5.453 \pm 0.212\%$, and $\Delta'^{17}O_{0.528} = 1.066 \pm 0.012\%$ (Figure 8). The data of the sample are consistent with data of ordinary chondrites, and the Haag analysis plots together with other LL chondrites close to the main field of other LL chondrites (Figure 8) and is similar to the O isotope composition of Stubenberg that fell several years before only 110 km away.

Titanium and Chromium Isotopes

The Ti isotope data show deficits in ϵ^{46} Ti and ϵ^{50} Ti (Table 4), which agree with data from the Parnallee ordinary chondrite (OC; LL3.6) and with the overall data of other OCs from the literature (Figure S5 in Supporting Information). Similarly, the ϵ^{53} Cr and ϵ^{54} Cr values (Table 4) overlap with data of OC reported in literature and are identical to that of Stubenberg (LL6) within analytical uncertainties (Bischoff et al., 2017). This consistency of Ti and Cr isotope data with those of OC data (Figure 8) demonstrates that Haag indeed belongs to the OCs.

Bulk Chemical Characteristics

For most elements, the chemical composition of Haag (Table 5; Figure 9) is close to the compositions of the analyzed LL chondrite breccias of Adzhi-Bogdo

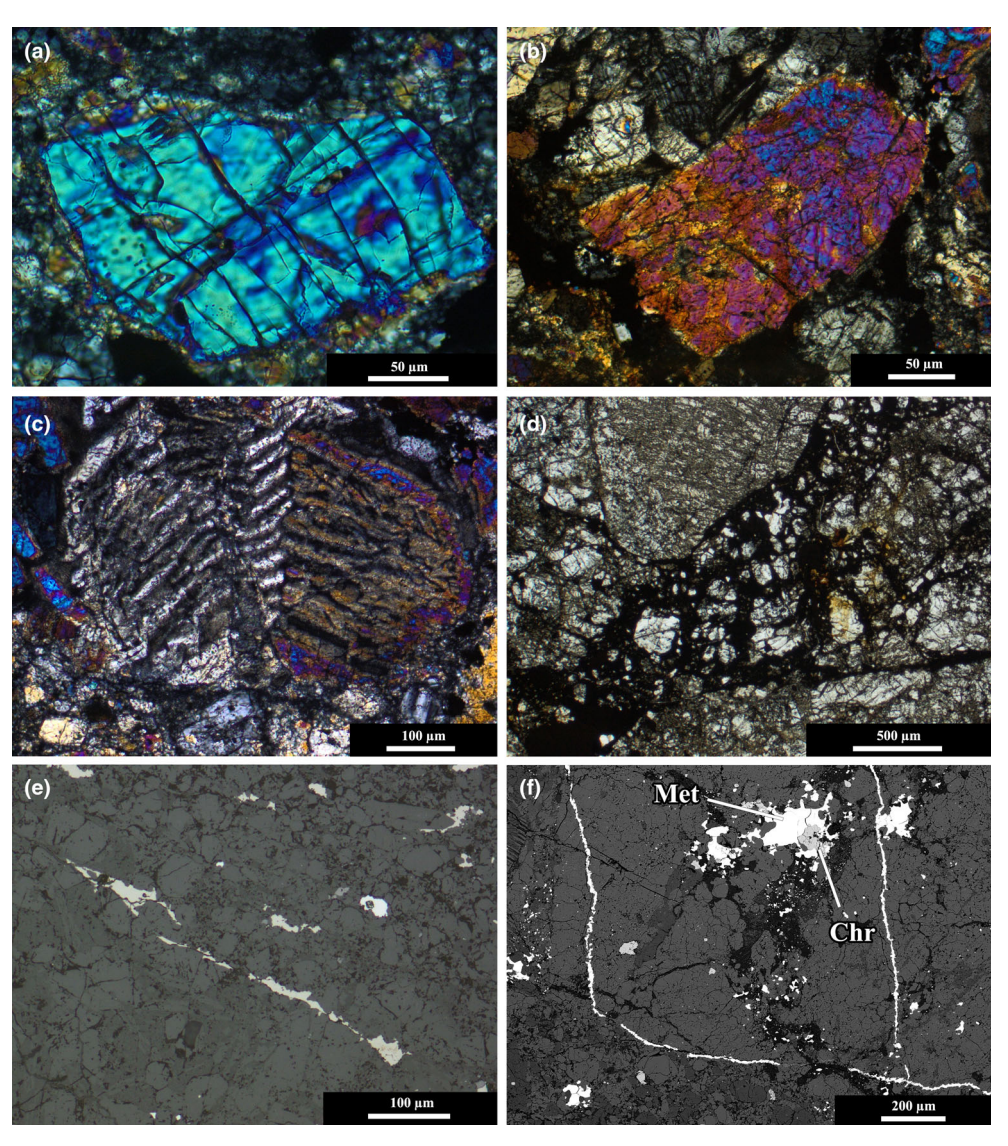


FIGURE 5. Shock effects in olivine vary from fragment to fragment. (a) Olivine with two sets of planar fractures; polarized light, crossed nicols. (b) A former large olivine grain shows strong mosaicism; polarized light, crossed nicols. (c) Shock-deformed barred olivine (BO) chondrule; polarized light, crossed nicols. (d) Part of a fragment with a shock-darkened area; plane polarized light. (e) Troilite-rich shock vein in reflected light. (f) Sulfide-rich veins (troilite), probably formed by impact deposition on cracks within an individual clast; Met = metals; Chr = chromite; BSE image.

and Stubenberg (Bischoff et al., 1993, 2017). It is also similar to the mean composition of LL chondrites (Lodders & Fegley, 1998). However, there are slight depletions in some elements (e.g., Co, Ni, Cu) as well as minor enrichments in Al, K, and P compared with the mean composition of LL chondrites, which will be discussed below.

Noble Gases

The noble gas results of the Haag analyses are summarized in Tables 6–8. The small sample Haag A of only ~1 mg was initially measured to probe for solar

wind. The data of all three Haag samples are largely consistent. The results of Haag B and C have lower uncertainties than those of Haag A, mainly due to lower blank corrections. Thus, in the following, we focus on the data obtained for the two larger samples, Haag B and C, and use an error-weighted mean of their ratios and concentrations to determine cosmic ray and gas retention ages. The Haag samples show a Ne composition within the typical cosmogenic range constrained in Wieler (2002; Figure S6 in Supporting Information). Thus, there is no indication for trapped (tr) Ne (nor He_{tr}). Instead, He and Ne are purely cosmogenic (cos) with additional radiogenic (rad) ⁴He_{rad}. Argon consists of a trapped

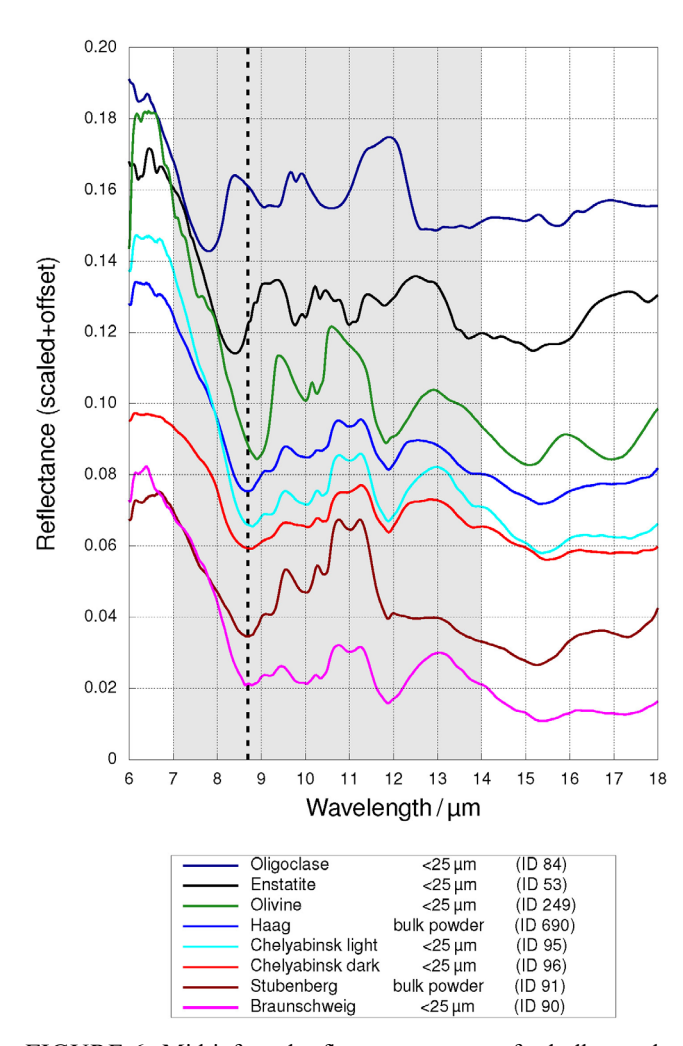


FIGURE 6. Mid-infrared reflectance spectra of a bulk powder aliquot of Haag (center; blue) compared with three pure minerals (top) and four meteorite spectra (bottom; Chelyabinsk (LL5-6) (two spectra), Stubenberg (LL6), Braunschweig (L6)) taken from the MERTIS IRIS infrared spectra database labeled with the ID under which each spectrum can be found (Weber et al., 2018). The dashed line indicates the Christiansen feature of Haag at 8.70 µm. The gray region indicates the measurement region of the MERTIS instrument onboard the BepiColombo spacecraft.

component in addition to Ar_{cos} (and $^{40}Ar_{rad}$) revealed by $^{36}Ar/^{38}Ar$ ratios (~2.4) that are higher than ($^{36}Ar/^{38}Ar)_{cos}$ (= 0.622–0.646; Figure S7 in Supporting Information). The origin of the Ar_{tr} cannot be resolved but is consistent with Q and air composition. The Kr and Xe compositions are likewise consistent with Q and air composition, with minor additions of (Kr, Xe)_{cos} and significant amounts of 129 I-derived 129 Xe.

Table 9 provides the cosmogenic noble gas concentrations and the shielding conditions for Haag within the meteoroid and corresponding production rate ranges P_x , and the calculated cosmic ray exposure (CRE)

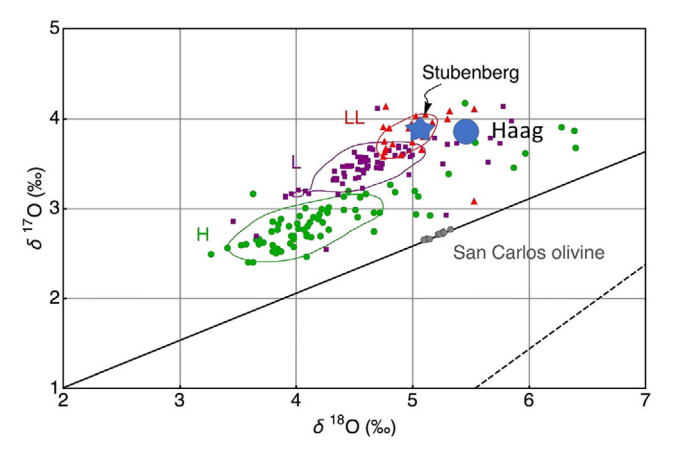


FIGURE 7. Plot of $\delta^{17}O$ versus $\delta^{18}O$ for Haag (circle) compared with those for Stubenberg (star) and other published oxygen isotope data for H, L, and LL ordinary chondrites. The results of San Carlos olivine standard measurements (gray filled circles) are displayed along with the terrestrial fractionation line (solid) and the carbonaceous chondrite anhydrous minerals mixing line (dashed). Modified figure from Bischoff et al. (2017).

ages T_x . Matches between measured (22 Ne/ 21 Ne)_{cos} and model predictions (Leya & Masarik, 2009; see S2-supplements) delivered possible preatmospheric meteoroid radii of 20–85 cm and a sample depth between 4 and 5 cm below the meteoroid surface. Two matches between measured and modeled data at unreasonably large radii (>300 cm, corresponding to a pre-atmospheric meteoroid mass of >360 tons using the density of Haag and assuming a spherical shape) and depths (>220 cm) were not considered.

Table 10 contains the radiogenic isotope concentrations and the U/Th-He and K-Ar gas retention ages.

Magnetic Susceptibility (χ) and Density

The magnetic susceptibility χ of three Haag specimens was analyzed in Nördlingen (Figure 10), producing values of $\log\chi=3.99$ (H01, 8.76 g), 4.065 (H02, 3.486 g), and 3.98 (H05, 64.06 g) with χ in 10^{-9} m³/kg, resulting in a weighted mean value of 3.99 \pm 0.05. The data indicate minor inhomogeneity. The bulk density values are 3.190 g/cm³, 3.187 g/cm³, and 3.194 g/cm³, respectively, that is, 3.190 g/cm³ on average. These results are well in the range of other LL chondrites (Rochette et al., 2003) and similar to those of Stubenberg (LL6 breccia) (Bischoff et al., 2017).

Helium pycnometry of specimen H02 provided a solid volume of $0.9975 \pm 0.0001 \, \mathrm{cm}^3$ and a corresponding grain density of $3.4945 \pm 0.0002 \, \mathrm{g/cm}^3$. The difference between the bulk and grain densities indicates an internal porosity of $\sim 8.8\%$.

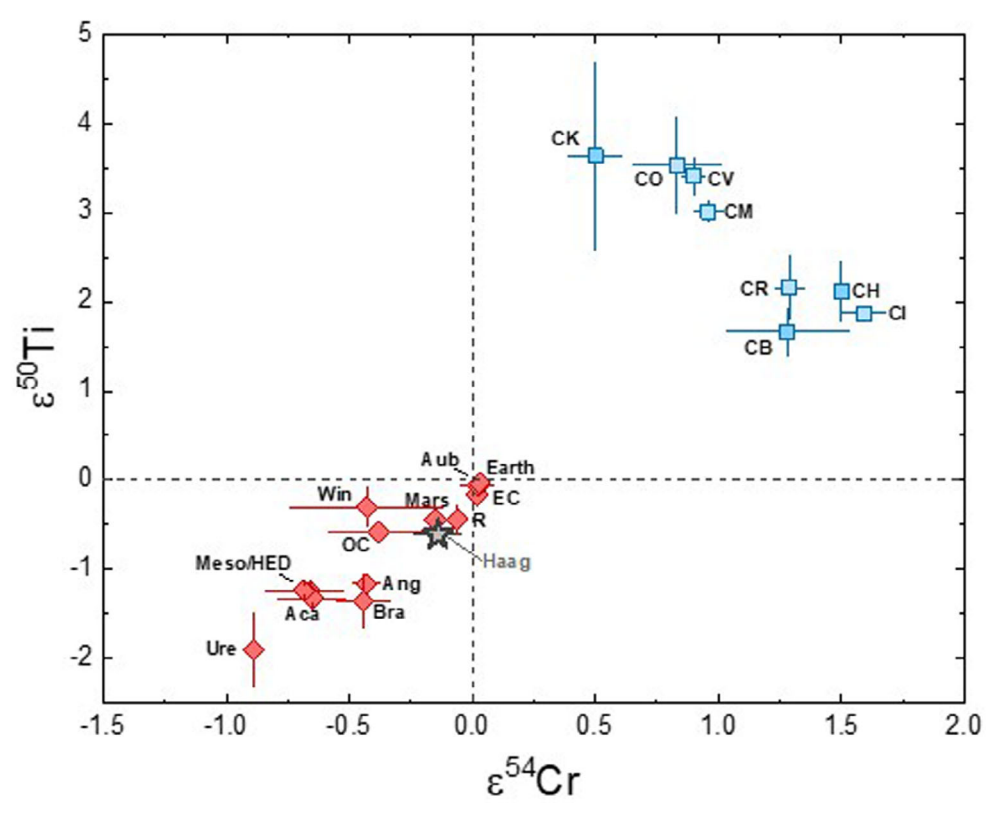


FIGURE 8. The Ti and Cr isotope data (Table 4) of Haag (gray star) overlap with the group average of ordinary chondrites (OC) within analytical uncertainty. Similar to Stubenberg, the ϵ^{54} Cr falls at the higher end of the distribution defined by previously reported OC data. The averages and corresponding uncertainties are from the compilation of Rüfenacht et al. (2023). Isotope data of the different carbonaceous chondrite groups are also presented. Aca, acapulcoites; Ang, angrites; Aub, aubrites; Bra, brachinites; EC, enstatite chondrites; IAB sil, IAB silicates; Meso, mesosiderites; NC, noncarbonaceous chondrites; R, R chondrites; Ure, ureilites; Win, winonaites.

TABLE 4. Nucleosynthetic Ti and Cr isotope data for Haag.

		•		-		-						
Sample	n	ε ⁴⁶ Ti	2 SE	$\epsilon^{48} Ti$	2 SE	ε ⁵⁰ Ti	2 SE	n	ε ⁵³ Cr	2 SE	ε ⁵⁴ Cr	2 SE
Haag	10	-0.23	0.07	-0.03	0.03	-0.61	0.07	14	0.35	0.06	-0.15	0.08
Stubenberg*	12	-0.08	0.11	-0.05	0.11	-0.67	0.09		0.43	0.03	-0.17	0.06
Parnallee	6	-0.08	0.08	0.01	0.07	-0.62	0.09					
BHVO-2	9	-0.06	0.09	0.05	0.07	0.04	0.07					
DTS-2								30	0.04	0.03	0.07	0.05

Note: n refers to the number of measurements. Isotopic values are averages of repeat measurements. Uncertainties are given in 2 SE (SE = SD/ \sqrt{n}). Parnallee (for Ti, sample solution from Rüfenacht et al. (2023)) and the terrestrial USGS magmatic reference samples BHVO-2 (for Ti) and DTS-2 (for Cr) were measured alongside Haag. (*) Data from Bischoff et al. (2017).

Short- and Long-Lived Radionuclides by Gamma Spectrometry

Seven cosmogenic radionuclides with half-lives between 27.7 d (⁵¹Cr) and 0.7 Ma (²⁶Al) were detected. Among those, four nuclides in Lab1 (at VKTA) and six nuclides in Lab2 (at TU Dresden) were above the decision threshold of the measurement method, and an activity could be quantified (Table 11; Figure 11). The decision threshold quantifies the physical effect of interest, which allows the conclusion that a physical effect is present or not.

Not clearly detectable, but recognizable, are other gamma energies of primordial and cosmogenic radionuclides whose mass-specific activity was too low to be evaluated. These include other secondary products from the natural ²³⁸U decay series as well as the cosmogenic nuclide ⁵⁷Co. In addition, traces of ¹³⁷Cs of anthropogenic origin were also visible below the decision threshold but probably arose from subsequent contamination at the site of discovery.

The specific activities of the natural decay series (Table 11) do not allow any statement to be made about

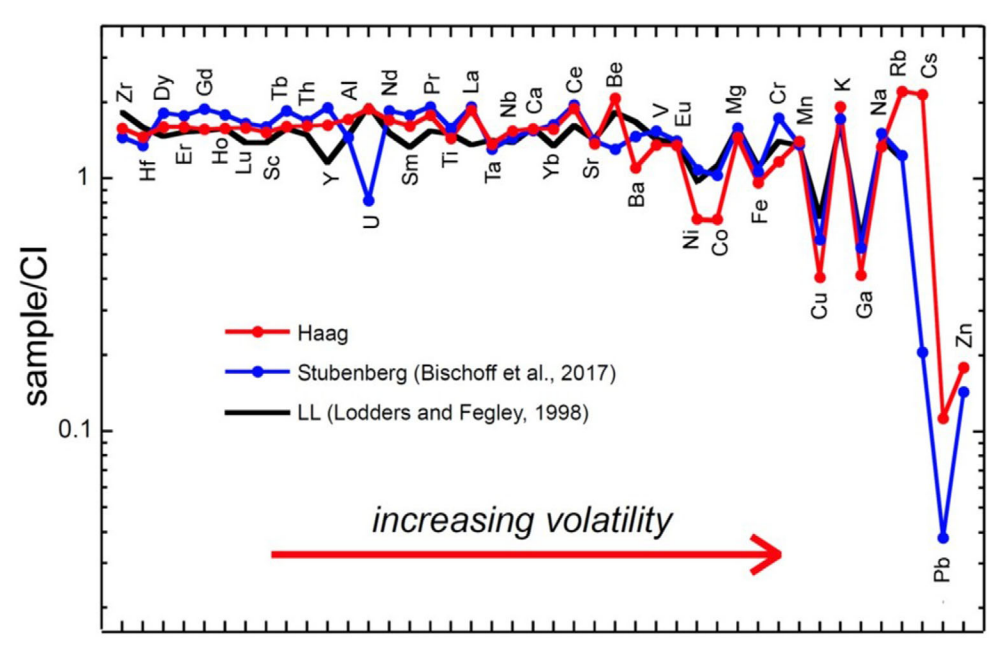


FIGURE 9. Element abundances relative to CI chondrites of Haag in comparison to the LL chondrite Stubenberg (Bischoff et al., 2017) and the average of other LL chondrites (Lodders & Fegley, 1998). For normalization, the CI values of Barrat et al. (2012) are used.

possible disequilibrium within the decay series. If, however, one assumes equilibrium of the decay series, terrestrial isotope ratios, and a homogeneous activity distribution in the sample, the element concentrations determined in Lab1 are 18 ± 8 ng/g (U), 94 ± 14 ng/g (Th), and 743 ± 129 µg/g (K), whereas those from Lab2 are 11 ± 3 ng/g (U), 69 ± 16 ng/g (Th), and 847 ± 88 µg/g (K).

Long-Lived Radionuclides by IAMS

The instrumental accelerator mass spectrometry (IAMS) determined nuclide ratios that can be explained by a relatively long CRE age (resulting in saturation of the respective radionuclide), that is, about 10^{-11} and 10^{-12} for $^{26}\text{Al}/^{27}\text{Al}$ and $^{41}\text{Ca}/^{40}\text{Ca}$, respectively (Table 12). Associated machine blanks were about three orders of magnitude lower, so no blank correction was applied to the results. No additional uncertainty was added to the specific activities to take into account for stable Al and Ca concentration value uncertainties.

Compositional Space in CHNOSMg of the Solvent-Soluble Organic Matter (SOM)

The organic matter (OM) content in meteorites may range from a few percent (2–4%) in CM and CI carbonaceous chondrites to lower values of ~0.5% in type 3 CV, CO, or OCs (Schmitt-Kopplin et al., 2012). With higher thermal metamorphism, organic matter will be

transformed and reduced gradually with increasing processing to lower values of ~0.25%, and among the SOM components, only the most thermostable organic fractions remain. Information on the abundance of SOM relative to and the total OM in a large set of meteorites is limited because of the small number of analyses and the small amounts of material. The mass spectrometry analysis of the methanol-SOM of Haag was performed following the same procedure as used earlier for the Stubenberg breccia (Bischoff et al., 2017). The main characteristic of the compositional space is a high density of m/z signals (with many signals in each nominal mass) over a mass range from 150 to 800 amu (Figure S8). This enormous number of m/z signals is annotated to more than 3000 molecular formulas with respect to C-, H-, N-, O-, S-, and Mg in their elementary composition. Majorly, the CHO, CHOMg, and CHOS compositions rule the detected soluble organic space of the Haag meteorite. The exact molecular formula assignments show a consistent coverage of ~3300 elementary compositions in the C, H, O, N, S, Mg compositional space (Figure 12).

DISCUSSION

General Remarks Based on Radionuclides

Nondestructive gamma spectrometry of the Haag meteorite sample was carried out between November 7 and November 25, 2024, over a total period of ~17.2 days in Lab1 and directly afterward between November 25,

14 A. Bischoff et al.

TABLE 5. Trace and major element abundances of Haag (H01; data in bold).

	Adzhi-	G. 1 1	**	
	Bogdo LL3-6	Stubenberg LL6 breccia	Haag LL4-6	Mean LL- chondrites
Element				
Si			18.5 ^b	18.9 ^a
Al	1.21 ^a	1.15 ^a	1.35 ^a	1.18 ^a
Fe	20.11 ^a	20.9 ^a	18.78 ^a	19.8ª
Mg	14.92 ^a	15.0 ^a	13.74 ^a	15.3 ^a
Na	0.725^{a}	0.73^{a}	0.64^{a}	0.684 ^a
Ni	1.27 ^a	1.23 ^a	0.775^{a}	1.06 ^a
P		1310	1061	910
S			2.05 ^b	2.1
K	470	913	1060	880
Ca	1.32 ^a	1.36 ^a	1.32 ^a	1.32 ^a
Sc	8.23	9.33	8.88	8.0
Ti		719	645	680
V	82.1	80.6	71.0	76
Cr	4460	4573	3065	3680
Mn	2430	2606	2685	2600
Co	587	536	359	480
Cu	140	73.1	51.6	85
Zn	70	43.54	54.4	56
Ga	4.3	5.06	3.94	5.3
Rb		2.88	5.18	2.2
Sr		10.88	10.6	13
Y		2.97	2.53	2.0
Zr		5.12	5.56	7.4
Nb	.0.0	0.42	0.44	0.150
Cs	< 0.2	0.039	0.41	0.150
Ba	0.22	3.6	2.71	4.0
La	0.23	0.451	0.437	0.330
Ce		1.17	1.13	0.880
Pr		0.175	0.162	0.130
Nd	0.17	0.858	0.789	0.650
Sm	0.17	0.272	0.246	0.205
Eu Gd	0.074	0.0825	0.079	0.078
Tb	0.042	0.387 0.0693	0.323 0.060	0.290 0.054
Dy	0.042	0.0693	0.406	0.054
Но	0.37	0.101	0.400	0.300
Er	0.069	0.101	0.069	0.082
Tm		0.234	0.200	0.240
Yb	0.19	0.0437	0.263	0.033
Lu	0.031	0.0405	0.203	0.230
Hf	0.051	0.0403	0.039	0.034
Ta	0.15	0.0193	0.130	0.170
W	0.82	0.121	0.0202	0.115
vv Pb	5.02	0.102	0.303	0.113
Th		0.0476	0.0455	0.047
U	0.011	0.0063	0.0435	0.015
		Bogdo (LL3-6) and		

Note: Data for Adzhi-Bogdo (LL3-6) and Stubenberg (LL6 breccia) are from Bischoff et al. (1993) and Bischoff et al. (2017), respectively. The mean concentration for the LL chondrites is from Lodders and Fegley (1998).

2024, and January 8, 2025, with a total counting time of 36.8 days, in Lab2 (Table 11). With a half-life of 53.22 d and 27.70 d, the short-lived cosmogenic radionuclides ⁷Be and ⁵¹Cr can serve as indicators of a fresh fall and, thus, as evidence of recent exposure to cosmic radiation. However, ⁷Be as a partial surface contamination (from atmospheric production), such as seen in Renchen (Bischoff, Barrat, et al., 2019), cannot be fully excluded. The results suggest that the sample from the Haag meteorite is a result of the bolide event over Austria on October 24, 2024. The ²²Na/²⁶Al ratios of Lab1 and Lab2, that is, 1.6 and 1.4, are close to the range of over one solar cycle averaged value of (1.7 ± 0.2) for L chondrites (Bhandari et al., 2002). Due to the relatively high uncertainty of 20% of the ²²Na activity in both laboratories, which is primarily based on the limited available size, the possible constraints concerning sample properties are limited. However, if the measured values are compared to radius- and depth-dependent (saturation) production rate calculations for ²²Na (Leya et al., 2021), smallest radii <8 cm can be excluded (Figure S9).

The U concentrations of Haag-01 are comparable to the one determined by ICP-SFMS (Table 5; 14.5 ng/g), whereas Th is higher and K is lower within 1-sigma uncertainty than 45.5 ng/g and 1060 ng/g (Table 5), respectively. The U, Th, and K element concentrations of the Haag chondrite (H01) can be compared to those found in the analyses of recent common L and LL chondrite cases, such as Stubenberg or Renchen (Bischoff et al., 2017; Bischoff, Barrat, et al., 2019). The U and K values are in good agreement with Renchen and Stubenberg. The Th value is twice as high in both comparative cases.

Mineralogical Properties and Classification of Haag

The chemical compositions of olivine and pyroxene suggest that Haag must be classified as an LL group chondrite. Based on the results presented in the Mineralogy and Petrology section, Haag is a breccia. The textures of most individual fragments are highly recrystallized (Figure 3), having only a few relic chondrules. The large grain size of plagioclase in many fragments (up to 300 µm; Figure 5) and the homogeneous compositions of olivines and pyroxenes support this. These facts clearly indicate that these fragments within Haag are of type 5 and 6. However, chondritic fragments also exist with well-defined chondrules and a fine-grained, feldspar-normative chondrule mesostasis. Olivine within these clasts is also equilibrated, as is typical for type 4 to type 6 chondrite lithologies. Overall, based on the mean olivine (Fa_{29,5±0.5}; range: 28–31 mol%; Table 1) and low-Ca pyroxene compositions (Fs_{23.9±1.4}Wo_{1.6±0.7}; range: 20-28 mol%; Table 1), the meteorite must be classified as an LL4-6 chondrite breccia. The slight variation of the

^aData in wt%; other data in $\mu g/g$ (ppm) measured by ICP-SFMS.

^bData in wt% obtained by electron microprobe (grid analysis).

ches Forschungszentrum, Wiley Online Library on [14/10/2025]. See the Terms and Conditions (https://onlinelibrary.wiley.com/terms -and-conditions) on Wiley Online Library for rules of use; OA articles are governed by the applicable Creative Commons License

TABLE 6. Helium and Ne concentrations (in 10^{-8} cm³ STP/g) and isotopic ratios in samples from H01.

			3 He/ 4 He x					
Sample	Mass [mg]	⁴ He	10^{4}	²⁰ Ne	20 Ne/ 22 Ne	21 Ne/ 22 Ne	$(^{22}Ne/^{21}Ne)_{\cos}$	$(^3\text{He}/^{21}\text{Ne})_{\cos}$
Haag A	1.076 ± 0.016	1585 ± 27	215.3 ± 5.2	6.96 ± 0.17	0.843 ± 0.013	0.863 ± 0.010	1.159 ± 0.014	4.74 ± 0.13
Haag B	14.519 ± 0.020	1496.3 ± 8.2	225.3 ± 1.6	6.497 ± 0.050	0.8228 ± 0.0026	0.8825 ± 0.0032	1.1331 ± 0.0041	4.839 ± 0.044
Haag C	14.239 ± 0.023	1468.7 ± 8.2	228.8 ± 1.8	6.406 ± 0.056	0.8280 ± 0.0039	0.8878 ± 0.0034	1.1263 ± 0.0044	4.893 ± 0.049
Haag mean						0.8850 ± 0.0023	1.1300 ± 0.0030	4.866 ± 0.033

Note: Also given are the sample masses from H01 used for noble gas analysis (He-Xe) and shielding-dependent cosmogenic isotope ratios. "Haag mean" is the error-weighted mean of Haag B and C (see text).

TABLE 7. Concentrations of Ar (in 10^{-8} cm³ STP/g) and Kr (in 10^{-10} cm³ STP/g) and isotopic ratios (84 Kr = 100) in samples from H01.

Sample	³⁶ Ar	36 Ar/ 38 Ar	$^{40}\mathrm{Ar}/^{36}\mathrm{Ar}$	⁸⁴ Kr	$^{78}\mathrm{Kr}/^{84}\mathrm{Kr}$	$^{80}{ m Kr}/^{84}{ m Kr}$	$^{82}{\rm Kr}/^{84}{\rm Kr}$	$^{83}{\rm Kr}/^{84}{\rm Kr}$	$^{86}\mathrm{Kr}/^{84}\mathrm{Kr}$
Haag A	3.19 ± 0.41	2.39 ± 0.35	2040 ± 280	4.3 ± 2.4	n.d.	7.5 ± 4.9	18 ± 14	19 ± 14	25 ± 22
Haag B	3.215 ± 0.049	2.397 ± 0.021	1911 ± 31	2.896 ± 0.036	0.891 ± 0.082	8.27 ± 0.19	22.77 ± 0.44	21.39 ± 0.35	29.61 ± 0.45
Haag C	3.255 ± 0.058	2.443 ± 0.034	1817 ± 34	2.31 ± 0.18	0.74 ± 0.11	9.09 ± 0.84	22.9 ± 2.3	21.8 ± 2.3	29.8 ± 3.4

TABLE 8. Xenon concentration (in 10^{-10} cm³ STP/g) and isotopic ratios (132 Xe = 100) in samples from H01.

Sample	¹³² Xe	124 Xe/ 132 Xe	$^{126}{\rm Xe}/^{132}{\rm Xe}$	$^{128}{\rm Xe}/^{132}{\rm Xe}$	$^{129}{\rm Xe}/^{132}{\rm Xe}$	$^{130}{\rm Xe}/^{132}{\rm Xe}$	$^{131}{\rm Xe}/^{132}{\rm Xe}$	134 Xe/ 132 Xe	$^{136}{\rm Xe}/^{132}{\rm Xe}$
Haag A	3.54 ± 0.58	0.51 ± 0.12	0.43 ± 0.16	9.0 ± 1.9	158 ± 31	16.5 ± 3.8	82 ± 19	43.2 ± 7.8	41.0 ± 7.3
Haag B	3.505 ± 0.021	0.459 ± 0.033	0.425 ± 0.024	8.41 ± 0.17	153.54 ± 0.96	16.41 ± 0.17	83.01 ± 0.73	37.54 ± 0.32	32.09 ± 0.36
Haag C	3.426 ± 0.050	0.519 ± 0.024	0.498 ± 0.018	8.36 ± 0.21	152.1 ± 2.5	15.69 ± 0.34	81.4 ± 1.6	38.33 ± 0.65	32.33 ± 0.59

Note: Tx ranges determined based on minimum and maximum cosmogenic isotope concentrations and production rates.

TABLE 9. Cosmogenic isotope concentrations (in 10^{-8} cm³ STP/g), shielding conditions (pre-atmospheric meteoroid radius and sample depth within the meteoroid), production rates P_x (in 10^{-8} cm³/(g × Ma)), and cosmic ray exposure ages T_x (in Ma).

Sample	3 He $_{\cos}$	²¹ Ne _{cos}	$^{38}\mathrm{Ar}_{\mathrm{cos}}$	Radius [cm]	Depth [cm]	P_3	P ₂₁	P ₃₈	T ₃	T ₂₁	T ₃₈	Preferred age
Haag A Haag B Haag C Haag mean	33.61 ± 0.19	7.12 ± 0.16 6.968 ± 0.055 6.869 ± 0.057 6.920 ± 0.039	0.819 ± 0.030	20-85	4–5	1.539–1.768	0.274-0.308	0.035-0.040	19–22	22–25	20–24	21–24

Note: Tx ranges determined based on minimum and maximum cosmogenic isotope concentrations and production rates.

low-Ca pyroxene is typical for pyroxene within type 4 fragments, which often show equilibrated olivine compositions and less equilibrated low-Ca pyroxene due to the faster equilibration process in olivines. However, in earlier classifications, chondrites with equilibrated olivines and slightly unequilibrated low-Ca pyroxenes were also classified as type 3.9 ordinary chondrites (e.g., Northwest Africa (NWA) 8031, Acfer 080; The Meteoritical Bulletin, 2025). Considering the Haag breccia, the occurrence of typical type 3 clasts with unequilibrated olivines and low-C pyroxenes in other parts of the rock cannot completely be ruled out.

For breccias, the fragment with the lowest degree of shock must be considered when determining the shock degree of the bulk rock. Thus, Haag has a shock degree of S2 (C-S2), considering the undulatory extinction of olivines in many lithic and mineral clasts (Bischoff,

Schleiting, & Patzek, 2019; Bischoff & Stöffler, 1992; Stöffler et al., 1991, 2018); although most fragments within Haag show shock features consistent with a higher degree of shock (S3 (C-S3) or S4 (C-S4)).

The Brecciation of Haag and its Noble Gas Characteristics

The noble gas analyses (see above) yield no trapped He and Ne, and the Ne isotopic composition is purely cosmogenic due to exposure of the meteoroid to galactic cosmic rays. Haag is thus not a regolith breccia, but it is a fragmental breccia instead. An origin of Haag from within the uppermost few centimeters of the meteoroid and parent body is very unlikely due to the absence of solar wind noble gases and no evidence for solar cosmic ray-derived Ne (see section on "Noble Gases" above). This is surprising since

1945010,0, Downloaded from https://onlinelibbrary.wiley.com/doi/10.1111/maps.70066 by Helmholtz Zentrum Menchen Deutsches Forschungszentrum, Wiley Online Library on [14/10/2025]. See the Terns and Conditions (https://onlinelibrary.wiley.com/terns-ad-conditions) on Wiley Online Library for rules of use; OA articles are governed by the applicable Creative Commons License

TABLE 10. Radiogenic isotope concentrations (in 10^{-8} cm³ STP/g) and U/Th-He and K-Ar gas retention ages $T_{\rm x}$ (in Ga).

Sample	⁴ He _{rad}	$^{40}\mathrm{Ar}_{\mathrm{rad}}$	T_4	T ₄₀
Haag A	1394 ± 32	6100 ± 1300		
Haag B	1306 ± 17	5750 ± 420		
Haag C	1279 ± 17	5510 ± 430		
Haag mean	1292 ± 12	5630 ± 300	~3.2	3.8-4.0

Note: The K, U, and Th concentrations used for chronology were taken from Table 5.

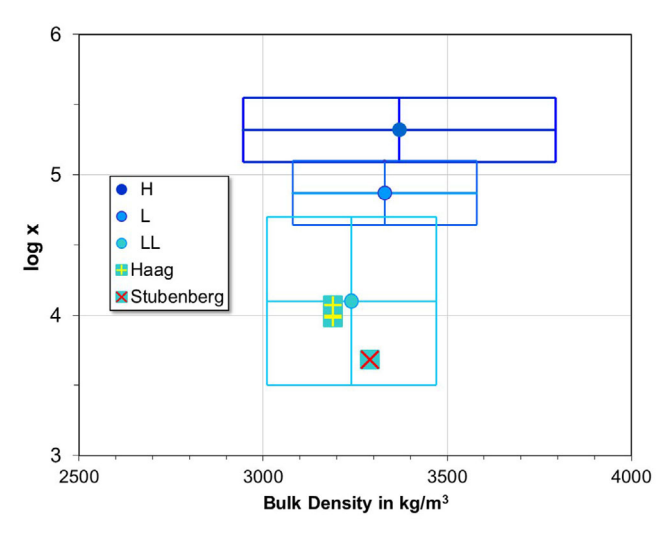


FIGURE 10. Illustration of the magnetic susceptibility and density of Haag. Haag has a magnetic susceptibility and density that plot in the range of other LL chondrites (Rochette et al., 2003). A similar value was obtained for Stubenberg (LL6) that fell only 110 km away some years before.

the clasts within the breccias point toward a complicated sequence of several impact events on the parent body. One possibility for a repeated impact process is shown in Figure 3e. The formation of the fine-grained constituents of the present clast would first require an impact event causing comminution of the target rocks and mixing of various rock components (silicates, sulfides (few metals)). A subsequent shock event would then be necessary for the lithification of the clastic material to form a fine-grained breccia. A third impact event would be needed for fragmentation of the fine-grained lithology and transport of the clasts to a location near the surface to be mixed with the other components of the Haag breccia (e.g., type 4-6 fragments (Figure 3a-c) and the impact-related brownish clast (Figure 5b)). All these fragments would then have to be shock-lithified by a fourth impact event to produce a solid, tough brecciated rock (Bischoff et al., 1983, 2006; Kieffer, 1975). A final collision would then be necessary to isolate the Haag meteoroid from the parent body, sending the ejected rock piece toward the Earth.

Considering brecciated chondrites for which noble gases have been analyzed, a remarkably high number (about 62%) of brecciated H chondrites contain solar noble gases compared to only around 11% and 10% of the brecciated L and LL chondrites, respectively (Bischoff et al., 2018).

Bulk Chemistry—Element Depletions and Enrichments

Comparing the Haag data with the mean composition of LL chondrites (Lodders & Fegley, 1998), we found similarities for most elements, but minor depletions exist in some elements (e.g., Co, Ni, Cu) as well as slight enrichments in Al, K, and P. It is difficult to consider the small depletions of Co, Ni, and Cu as a sampling effect since a large bulk sample of about 0.6 g was homogenized, from which the aliquot was taken for bulk chemical analysis. Since the Haag sample is heavily brecciated, it is obvious that the sample experienced extreme modification processes in the near-surface region of the parent body. The repeated impact fragmentation and mixing have probably also led to a redistribution of chondrite constituents. Such a process may be responsible for causing a slight separation of the higher density components (metals, sulfides) relative to the constituents with lower density (mostly silicates). After lithification of the loose materials to form the heavily fragmented breccia (Bischoff et al., 1983; Kieffer, 1975), the parent body material from which Haag (LL4-6) resulted was slightly depleted in the densest constituents (especially metals). This impact-related reason for the Co, Ni, and Cu depletion is also consistent with the analyses of two impactproduced fragments shown in Figures 3e and 5b, which are strongly depleted in Ni (Table 3). We cannot expect that the above-discussed process has affected all types of breccias. Monomict breccias like Stubenberg (LL6) certainly formed without complex mixing of various types of clasts.

The Haag chondrite contains small, probably impact-related particles that are chemically rich in Al, Cr, and Ca (Figure 5b; Table 3). The presence of these objects might be the main reason for the slightly elevated Al concentration in the bulk rock composition (Table 5). Compared with the mean composition of LL chondrites, Haag has a minor enrichment in P that is related to the abundance of phosphates in the sample. Since Haag obviously is a very complex breccia, this observation might be a good reason that we cannot explain all enrichments and depletions in more detail.

Implications of Spectroscopic Measurements for Remote Sensing

The wavelength of the CF at 8.70 µm (1149 cm⁻¹) is located between the CFs of the two most abundant minerals in Haag—olivine and pyroxene—and, therefore,

19455100, 0, Downle aded from https://onlinelibrary.wiley.com/doi/10.1111/maps.70060 by Helmholtz Zentrum Muenchen Deutsches Forschungszentrum, Wiley Online Library on [14/10/2025]. See the Terms und-conditions) on Wiley Online Library for rules of use; OA articles are governed by the applicable Creative Commons Licenso

TABLE 11. Specific activities of radionuclides determined in Haag by gamma spectrometry compared with those determined in recent falls of similar chemical composition.

Specific activity [dpm/kg]	Half-life	Haag VKTA Lab1	Haag TU Dresden Lab2	Renchen (R2)	Stubenberg (M1b)
Cosmogenic					
⁷ Be	53.2 d	84 ± 25	73 ± 12	150 ± 6	74 ± 10
²² Na	2.60 a	96 ± 19	89 ± 18	106.7 ± 1.3	87 ± 9
²⁶ A1	$7.05 10^5 a$	45 ± 9	50 ± 10	65 ± 7	61 ± 5
⁴⁶ Sc	83.8 d	<7.2	5.1 ± 1.3	11.1 ± 1.2	7.6 ± 0.8
⁵¹ Cr	27.7 d	< 78	36 ± 14	59 ± 11	32 ± 9
⁵⁴ Mn	312.2 d	63 ± 10	51 ± 5	85 ± 9	55 ± 6
⁵⁷ Co	271.8 d	<5.3	<1.4	9.5 ± 1.3	4.9 ± 0.9
Primordial					
²³⁸ U chain	4.47 10 ⁹ a	13 ± 6	8.3 ± 2.2	11.9 ± 0.7	11.9 ± 1.5
²³² Th chain	14.0 10 ⁹ a	23 ± 9	16 ± 4	10.7 ± 0.7	8.5 ± 0.7
40 K	1.25 10 ⁹ a	1380 ± 221	1573 ± 157	1923 ± 115	1540 ± 148

Note: All activity data are referenced to the date of the respective falls, that is, March 6, 2016 (Stubenberg (LL6); M1b; Bischoff et al., 2017), July 10, 2018 (Renchen (L5-6); R2; Bischoff, Barrat, et al., 2019), and October 24, 2024 (Haag). Half-lives are from the C.E.A. Laboratoire National Henri Becquerel, Decay Nucléide—Lara Library for gamma and alpha emissions (www.lnhb.fr/Laraweb/index.php) and for ²⁶Al Norris et al. (1983). Secular equilibrium assumed for U and Th decay chains. Uncertainties given as 68% CL; limits given as 90% CL.

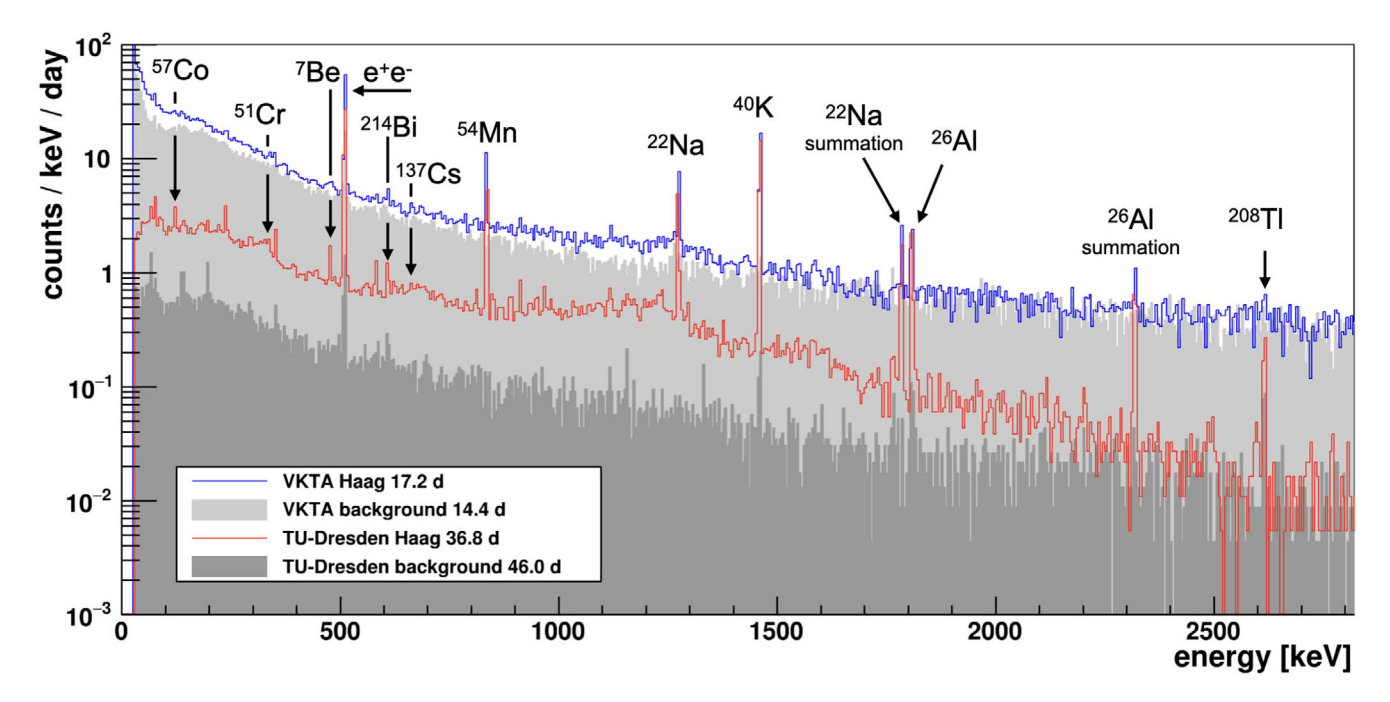


FIGURE 11. Gamma-ray spectra measured at VKTA (Lab1 in blue; top line) and TU Dresden (Lab2 in red; bottom line), respectively, of the \sim 6 g Haag meteorite (H01) along with background spectra of each detector (shades of gray). The gamma lines detected from members of the natural decay chain of the primordial nuclides 238 U and 232 Th as well as 40 K (Table 11) and short- and long-lived cosmogenic nuclides are labeled.

TABLE 12. Nuclide ratios measured by IAMS and resulting specific radionuclide activities, based on ²⁷Al and Ca from Table 5, in Haag (H01). Total uncertainties also include those from the standards.

	$^{26}\text{Al}/^{27}\text{Al}$	26 Al (dpm kg $^{-1}$)	41 Ca/ 40 Ca	⁴¹ Ca (dpm kg ⁻¹)
Haag Blank	$(8.72 \pm 0.29) \times 10^{-12}$ $(8.9 \pm 3.0) \times 10^{-15}$	49.2 ± 1.6	$(2.15 \pm 0.35) \times 10^{-12}$ <8 × 10 ⁻¹⁵	5.25 ± 0.86

19455100, 0, Downloaded from https://onlinelibrary.wiley.com/doi/10.1111/maps.70060 by Helmholtz Zentrum Muenchen Deu

zentrum, Wiley Online Library on [14/10/2025]. See the Terms and Condit

onditions) on Wiley Online Library for rules of use; OA articles are governed by the applicable Creative Commons Licenso

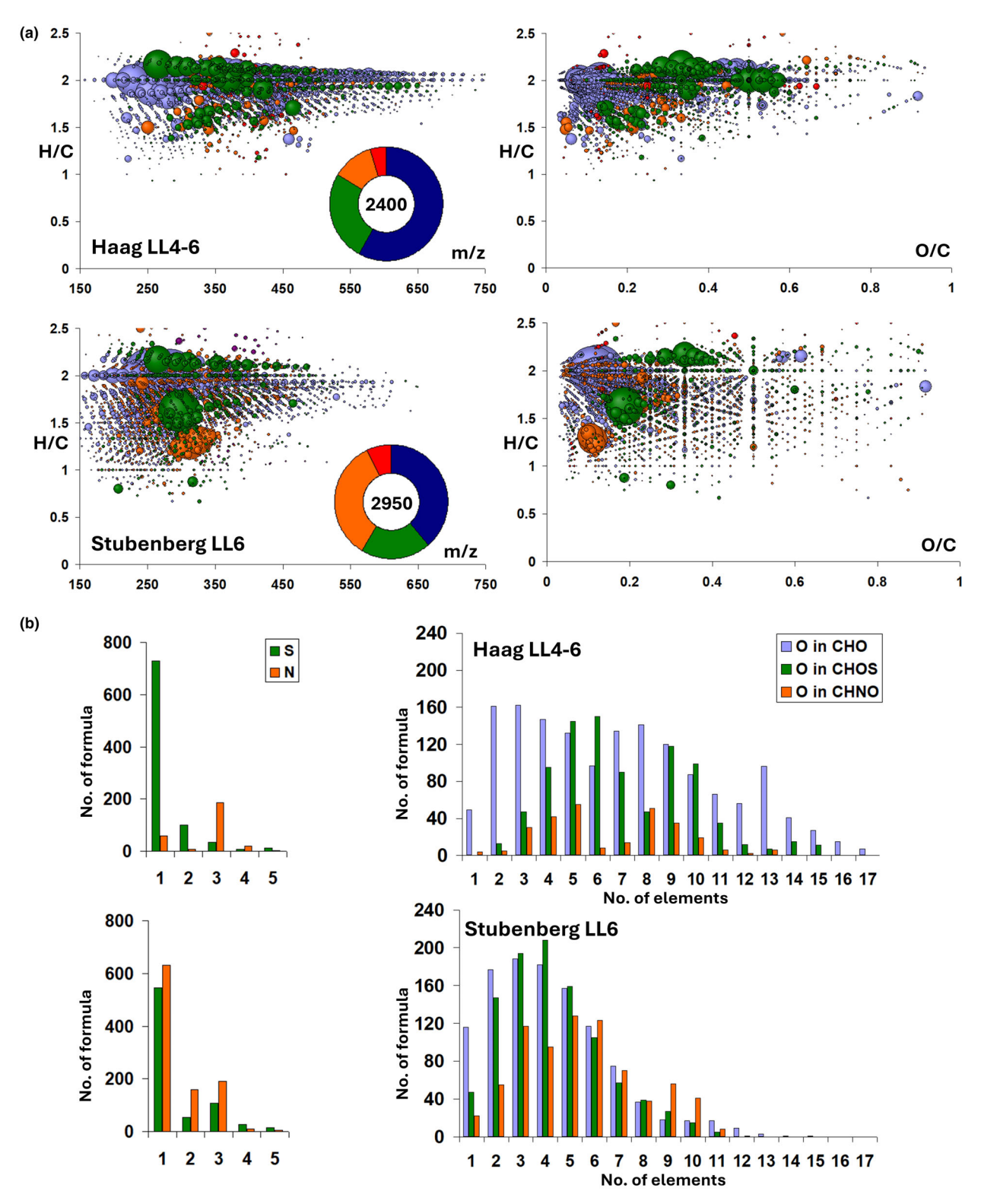


FIGURE 12. Compositional space in CHNOS of the Haag meteorite compared to that of the Stubenberg chondrite. (a) The van Krevelen diagrams illustrate the saturation degree (H/C) of the detected molecules as a function of their molecular size (m/z) and their oxidation state (O/C). (b) The abundance of formulas with various heteroatom numbers (S, N) and oxygens in the CHO, CHNO, and CHOS series are described, clearly showing higher oxygenations of molecules in Haag compared to Stubenberg. The peak intensity in the mass spectra is shown as the bubble size; the color follows the rules whereby blue is for CHO, green for CHOS, orange for CHNO, and red for CHNOS.

essentially displays the mixture of both minerals (Figure 7) (e.g., Morlok et al., 2023; Weber et al., 2021). In addition, the CF wavelength is in the expected range for LL chondrites (Salisbury et al., 1991). Even though a significant amount of sample material is plagioclase (~10 vol%), the wavelength of the CF seems to be unaffected by this. The CF wavelengths of plagioclases with comparable chemical composition are clearly shorter than 8 μ m (1250 cm⁻¹) (Reitze et al., 2021a).

In addition, it is known that plagioclase spectral bands in mineral mixtures are often subdued or even invisible (e.g., Weber et al., 2023). However, the CF is not the global minimum in the investigated wavelength region, as was expected. Instead, the region of the CF shows an increased reflectance. We suggest that this is the contribution of the underlying plagioclase signal (Reitze et al., 2021a).

The RBs are also located at the expected values for a mixture of olivine and pyroxene. However, the overall intensity of the bands is diminished in comparison to the pure mineral spectra. As the wavelength of the CF does not directly show the influence of the plagioclase component, the RBs also seem unaffected, as bands of plagioclase with comparable chemical compositions (Reitze et al., 2021a) are not directly observable in the Haag spectrum.

The TF might be more affected by the pyroxene component and probably the plagioclase component, although both have a lower concentration within the meteorite. This indicates that pyroxene and plagioclase are enriched in the finer fractions of the sample aliquot due to grinding of the bulk rock (cf. Reitze et al., 2021b).

Upon comparing Haag with the two Chelyabinsk (LL5-6) lithologies and with Stubenberg (LL6) as well as Braunschweig (L6; Figure 7), we see that the CF of the first three is comparable to Haag's CF, whereas the CF of Braunschweig does not match (Bischoff et al., 2017; Bartoschewitz et al., 2017; Morlok et al., 2017). The deviation between the CFs of the Haag and Braunschweig spectra might be related to the powder fractions. Grinding and sieving of feldspar-containing rocks like lunar rocks are known to be enriched in feldspar in the finest fraction (e.g., Taylor et al., 2001). Therefore, the small tip in the Braunschweig spectrum might represent the more strongly enriched plagioclase component. In turn, the fact that there is no clear identification of plagioclase in the Haag spectrum suggests that either the feldspar enrichment is smaller or Haag experienced stronger space weathering that also led to disappearing bands due to loss of crystallinity (e.g., Weber et al., 2023).

The RBs of Chelyabinsk have a lower relative intensity compared to those of Haag (Figure 7), which might have arisen from the higher shock that Chelyabinsk experienced in comparison to Haag (cf.

Morlok et al., 2017). The TF of Haag is more similar to that of the Chelyabinsk dark lithology than to that of the Chelyabinsk light lithology, which indicates that the finest fraction of Chelyabinsk dark lithology has a more similar mineralogy composition to Haag than does the light lithology fraction, also confirming the lower degree of shock Haag experienced.

The spectra of the Stubenberg and Braunschweig meteorites (Bartoschewitz et al., 2017; Bischoff et al., 2017) show RBs at similar wavelengths to Haag, indicating a comparable mineralogy composition. However, the TF of Braunschweig (L6) is shifted toward longer wavelengths compared to that of Haag (LL4–6), which might be because of the different olivine to pyroxene ratios between L and LL chondrites (Dunn et al., 2010), perhaps in combination with an increased plagioclase abundance in the finest fraction (<25 µm in Braunschweig; Figure 7).

As the average grain size of lunar regolith is between 60 µm and 80 µm, and asteroid and other planetary regolith is also expected to be in this grain size range, the TF is an important property for interpreting remote sensing data (e.g., Heiken et al., 1991; Reitze et al., 2021b; Vernazza et al., 2012, and references therein). Our data confirm that the grinding of rocks—on planetary objects as well as in the laboratory—leads to changes in the modal composition of different minerals (Reitze et al., 2021b; Taylor et al., 2001). This observation is important for midinfrared remote sensing analyses of meteorite parent bodies and other planetary objects, as the wavelength of the TF can display a mineralogic composition other than that of the RB. In addition, the observation that the spectral region of the CF might be affected by the plagioclase component, which is otherwise almost invisible, even in spectra with higher plagioclase content, is important for the upcoming MERTIS instrument to Mercury, which measures between 7 µm and 14 µm, as Mercury's northern smooth plains are likely to be rich in plagioclase, with a chemical composition comparable to that of LL chondrites (Hiesinger et al., 2020; Namur & Charlier, 2017; Weber et al., 2023).

Significance of Noble Gas Studies and Implications for the Irradiation History

Pre-Atmospheric Meteoroid Size, Sample Shielding, and CRE Ages

The T_x ranges determined based on the different cosmogenic noble gas isotopes overlap. The T_3 range is slightly lower than the T_{21} and T_{38} ranges, which are remarkably consistent. We can exclude significant ^3He loss due to heating, for example, during atmospheric entry and preferentially affecting the lighter noble gases, as the Haag data plot on the trend of OCs in a cosmogenic $^3\text{He}/^{21}\text{Ne}$ versus $^{22}\text{Ne}/^{21}\text{Ne}$ diagram (see

"Bern plot," Nishiizumi et al., 1980; Figure \$10 in Supporting Information). It has been suggested that an overestimation of P₃ in the model is responsible for the relatively low T₃ (Bischoff, Patzek, Alosius, et al., 2024; Bischoff, Patzek, Barrat, et al., 2024). We find a discrepancy of ~11% in the (3He/21Ne)cos ratio between modeled and measured chondrite data for a (²²Ne/²¹Ne)_{cos} ratio of ~1.13 as measured in Haag by comparing with Dalcher et al. (2013; cf. Figure 1). Lowering P₃ accordingly results in a T₃ of 21-25 Ma, which is perfectly consistent with T_{21} and T_{38} . Our preferred CRE age for Haag is 21-24 Ma. This is within the (fairly large) CRE age range of LL chondrites (\sim 0.5–80 Ma), between the strongest peak at \sim 15 Ma and a broader peak at 27-33 Ma in the CRE age distribution (Graf & Marti, 1994; Herzog & Caffee, 2014). Note that these ages are determined with distinct production rate schemes, which may result in minor absolute age deviations.

Further Constraints on Pre-Atmospheric Radius and Shielding Depths by Cosmogenic Radionuclides

The 26 Al value of H01 from IAMS (49.2 \pm 1.6 dpm/kg) is in excellent agreement with both 26 Al values from gamma spectrometry (45 \pm 9 and

 50 ± 1.6 dpm/kg, respectively) (Figure S11). This has also been demonstrated for Elmshorn (Bischoff, Patzek, 2024) Alosius. et al.. and Ribbeck (Bischoff, Patzek, Barrat, et al., 2024). The comparison (Figure 13) of the IAMS ²⁶Al with radius- and depth-dependent (saturation) production rate calculations, developed for L chondrites (Leva et al., 2021), lets us exclude preatmospheric radii of up to 10 cm. The H01 sample was exposed to cosmic rays at a rather shallow depth ≤ 12.5 cm. The comparison of Haag's ⁴¹Ca data with calculations by Leya and Masarik (2009) developed for ordinary chondrites and also adapted for Haag's chemical composition indicates radii smaller than 80 cm and shielding depth < 50 cm. Hence, both IAMS-nuclide data are consistent with the noble gas results (Figure 13).

U/Th-He and K-Ar Gas Retention Ages

As presented in Table 10, the T_4 age (~3.2 Ga) is younger than the T_{40} age (3.8–4.0 Ga), which is commonly observed and explained by (multiple) smaller, for example, impact-induced, resetting and degassing events on the parent body, preferentially affecting the likely less retentive ${}^4He_{rad}$ compared to ${}^{40}Ar_{rad}$ (Bischoff, Patzek, Barrat, et al., 2024; Brown et al., 2023; Váci et al., 2020).

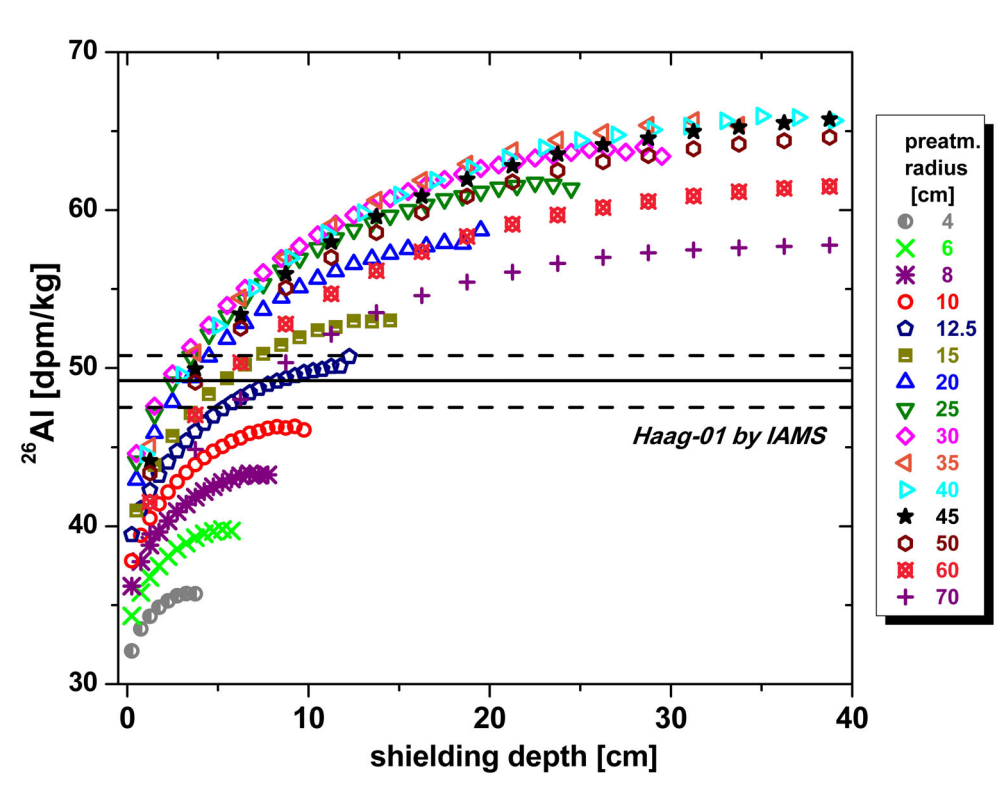


FIGURE 13. The ²⁶Al-specific activity of Haag-01 (H01; black line) calculated from IAMS data with 1-sigma uncertainties (black dotted lines) compared to radius- and depth-dependent (saturation) production rate calculations for ²⁶Al for L chondrites (Leya et al., 2021). The production rates are based on the chemical composition in Table 5.

Implications of the soluble organic compositions for the meteorite's thermal and impact processing

As shown above, the main characteristic of the compositional space is a high density of m/z signals over a mass range from 150 to 800 amu (Figure S8), with higher masses than the profile of Stubenberg. The chemical space is plotted in van Krevelen-type diagrams as H/C versus O/C ratio or m/z ratio (Figure 12), keeping the abundances of the mass spectra signals proportional to the bubble sizes. This allows insights into the chemical properties of the complex mixtures from the plotted chemical compositions. Information regarding the degree of unsaturation and oxygenation of the respective chemical compositions is described with the H/C and O/C ratios, respectively. As for the Stubenberg breccia, the Haag soluble organic matter shows a broad range of oxygenation of mainly aliphatic compounds, very representative of stony chondrites (e.g., et al., 2017; Ruf et al., 2017; Schmitt-Kopplin et al., 2012). Haag is an LL4-6 chondrite whose bulk sample shows an organics mixture that has been submitted to both low (type 4) and high (type 6) metamorphism levels: this differs from the Stubenberg breccia (LL6), whose fragments only saw the highest metamorphism level (type 6). The Haag meteorite is rich in sulfurized molecules, depleted in nitrogen compounds and is much more aliphatic in structure than Stubenberg, which has many highly condensed polyaromatic structures that are absent in Haag. The main difference is in the oxidation profile of Haag, shown in Figure 12 with a bimodal distribution of oxygen in all CHO, CHNO, and CHOS chemical families, probably reflecting the LL4 and LL6 types as a mixture, whereas Stubenberg contains many less oxygenated compounds typical of higher thermal metamorphism and water loss in LL6 type. Haag and highly Stubenberg show nitrogenated compounds (Jenniskens et al., 2014; Popova et al., 2013), reflecting a shock stage of Haag (S2; also having S3 and S4 fragments) relative to Stubenberg (S3). This is also visible in the close and complete profiles of organomagnesium compounds (CHOMg) in both meteorites, Stubenberg having more than 1000 CHOMg compositions compared to 800 for Haag (Figure S12). Considering that both are similar LL chondrites, this may reflect a slightly higher metamorphic temperature and a complex shock history of the Stubenberg parent body, as these thermostable metalorganic compounds could be related to the degree of a meteorite's thermal process (Ruf et al., 2017). From the rapid results obtained on the soluble organic compositions, we can conclude that the Haag (LL4-6) signature is very consistent with the profiles of the Stubenberg (LL6) breccia and shows characteristics consistent with the complex shock, brecciation, and lithification history of breccias.

Haag and the History of Austrian Meteorites

The first fall in Austria—observed and retrieved dates back to the year 1768 (Mauerkirchen, Upper Austria: mass: approx. 19 kg). It then took almost another 150 years before a second fall was witnessed and documented (1905: Minnichhof, Burgenland; mass: 550 g). The 1905 meteorite fall was quickly followed by Lanzenkirchen (1925, Lower Austria; mass: approx. 7 kg) and Prambachkirchen (1932, Upper Austria; mass: 2.1 kg). The casual discovery of the meteorite Ischgl 1976 (listed as a meteorite find of approx. 0.72 kg in the Meteoritical Bulletin Database, 2025) in Tyrol could be recognized by a study (Gritsevich et al., 2024) as a photographically registered meteorite fall of the year 1970. The last fall featured in the Austrian meteorite collection of the Natural History Museum (NHM) Vienna is the hard-to-find Kindberg (L6; Gattacceca et al., 2022). It fell in November 2020 but was recovered about 9 months later, in July 2021 (mass: 233 g) on a private Styrian forest road. Aside from the falls and Ischgl, two finds have also been recognized: Mühlau (1877, Tyrol; mass: 5 g) and Ybbsitz (1977, Lower Austria; mass: approx. 15 kg). Ybbsitz (H4) was found by students during field work and studied in great detail (e.g., Bischoff, 1985; Brandstätter et al., 1985; Palme et al., 1985). The trace element compositions of rare Al-rich chondrules within Ybbsitz (H4) were later studied by Instrumental Neutron Activation Analysis (INAA; **Bischoff** et al., 1989). More details on Austrian meteorites are presented in the Meteorite Bulletin Database (https:// www.lpi.usra.edu/meteor/).

A Remarkably High Number of Recovered Meteorite Falls in Central Europe

Including the Haag meteorite fall, a total of 13 meteorite falls have been recovered in an area with less than a 500-km radius (with an incidental center near Leipzig (Germany); Figure 14) since the Braunschweig fall (L6; Bartoschewitz et al., 2017) in April 2013. Such a high rate of recovered samples is certainly (at least in part) related to the successful work of the European Fireball Network and the excellent initiatives of the American Meteor Society (AMS; https://www.amsmeteors.org/) and the International Meteor Organization (IMO; https://fma.imo.net), which have motivated private search and recovery campaigns and increased their success rates.

FIGURE 14. Including the Haag meteorite, 13 meteorite falls have been recovered in an area with less than a 500-km radius since the Braunschweig fall (L6) in April 2013. The center is located near Leipzig (Germany).

Haag (LL4-6) represents the third LL chondrite in the above-mentioned area that has been identified, whereby the other two are Stubenberg (LL6; Bischoff et al., 2017; Ebert & Bischoff, 2016b; Spurný et al., 2016) and Hradec Králové (LL5; 2016; Gattacceca et al., 2019). Of the 13 meteorite falls in this area, these three LL chondrites represent a high percentage (23%) of the overall falls. Typically, just 8.5% of meteorite falls (112) of 1315 (excluding doubtful falls); The Meteoritical Bulletin, 2025, May 6) are LL chondrites. It is remarkable that the two LL chondrites Haag and Stubenberg fell within a short time close to each other. Similarly, Wethersfield (1982) fell in the same town in Connecticut as Wethersfield (1971), but 11 years later. Both are L6 chondrites (The Meteoritical Bulletin, 2025, August 1).

Eleven of these 13 falls are ordinary chondrites; the other two are the C1 chondrite Flensburg (Bischoff et al., 2021) and the Ribbeck aubrite (Bischoff, Patzek, Barrat, et al., 2024).

Considering the recent fall statistics for the area discussed above, it is remarkable that between the Neuschwanstein meteorite fall (EL_a6) in April 2002 (Weyrauch et al., 2018; Zipfel et al., 2010) and Braunschweig (L6; Bartoschewitz et al., 2017) in April 2013, no meteorite had been recorded for 11 years. But starting with Braunschweig (2013), six falls occurred in Germany during the following 11 years: Stubenberg (LL6; Bischoff et al., 2017; Ebert & Bischoff, 2016b; Spurný et al., 2016), Renchen (L5-6; Bischoff, Barrat, et al., 2019), Flensburg (C1; Bischoff et al., 2021), Elmshorn (anomalous H3-6; Bischoff, Patzek, Alosius, et al., 2024), and Ribbeck (aubrite; Bischoff, Patzek, Barrat, et al., 2024), two in Czechia (Hradec Králové (LL5; 2016; The Meteoritical Bulletin, 2025), and Zd'ár nad Sázavou (L3; Spurný, 2016; Spurný et al., 2016), and two in Austria (Kindberg (L6, 2020; Bischoff et al., 2025; Gattacceca et al., 2022) and Haag (this study); Figure 14)). In addition, the falls of Broek in Waterland (L6, 2017; Gattacceca et al., 2019), Ejby (H5/6; Haack et al., 2019; Spurný et al., 2017), and Antonin (Bischoff et al., 2022; Shrbeny et al., 2022) were reported in neighboring countries (The Netherlands, Denmark, and Poland, respectively; Figure 14).

1945510.00, Dowloaded from https://onlinelbhary.wiley.com/doi/10.1111/maps.70060 by Helmholtz Zontrum Menchen Deutsches Forschungszentrum, Wiley Online Library on [14/10/2025]. See the Terms and Conditions (https://onlinelbhary.wiley.com/ems-ad-conditions) on Wiley Online Library for rules of use; OA articles are governed by the applicable Centure Commons License

CONCLUSIONS

The detection of short-lived radionuclides from a small Haag meteorite sample measured shortly after its recovery confirms that Haag is the sixth recovered meteorite fall in Austria and connected with the bolide fireball event from October 24, 2024.

The rock is a severely fragmented ordinary chondrite breccia and consists of typical equilibrated and recrystallized lithologies with olivine and pyroxene compositions typical for LL chondrites (LL4-6). The petrologic and chemical properties of some clasts confirm a complex history of the bulk rock with multiple processes of impact-related brecciation, mixing, and lithification.

The LL chondrite classification is supported by O, Cr, and Ti isotope data, the results of bulk chemical analysis, as well as by physical properties like density and magnetic susceptibility.

Haag does not contain detectable concentrations of solar wind-implanted noble gases, and therefore, we can rule out a long exposure at the direct surface of the parent body.

LL chondrites are relatively rare among ordinary chondrites: Considering all meteorite falls, only 8% are LL chondrites. Therefore, it is remarkable to have two LL chondrite falls within 8 years in close proximity to each other (within 110 km).

Acknowledgments—We thank the two reviewers Alan Rubin and Rhian Jones and the Associate Editor Josep Trigo-Rodriguez very much for their great work, support, and time in order to improve the quality of this manuscript. We also thank U. Heitmann (Münster), W. Wegner, and G. Batic (both Vienna) for sample preparation and technical assistance, Celeste Brennecka for editorial support, Benjamin Rudelstorfer for providing meteorite specimens (H02, H05) for our scientific work, and Jarosław Morys for two pictures of meteorite (H02). We further acknowledge the help of members of Fa. Digimold Reverse Engineering (D-96515 Sonneberg, Germany), who digitalized the smallest meteorite sample, and we thank Robert Horny from the Institute for Materials Resource Management (MRM) of the University of Augsburg (Germany) for Helium pycnometry and for performing and analyzing the CT scan, and Armin Kriele from the German Engineering Materials Science Centre (GEMS) at the Helmholtz-Zentrum Hereon (D-85747 Garching, Germany) who digitalized the largest meteorite sample. We further acknowledge the VERA Team, especially Peter Steier, Stephanie Adler, and Carlos Vivo Vilches, for their analytical support and discussions. The VERA "cosmogenics" team was supported by the ChETEC- INFRA (Horizon 2020, No. 101008324) grant. M. P. R. and I. W. are supported by the DLR funding 50QW2502A in the framework of the BepiColombo mission. This work has partially been carried out within the framework of the NCCR PlanetS supported by the Swiss NSF (Swiss National Science Foundation) under 51NF40_205606 (M.S.) and grant SNF_219860 (D.K). Open Access funding enabled and organized by Projekt DEAL.

Data Availability Statement—All infrared data are free of charge and without registration available in the MERTIS IRIS Infrared database http://bc-mertis-pi.uni-muenster.de/.

Editorial Handling-Josep M. Trigo-Rodríguez

REFERENCES

- Barrat, J.-A., Gillet, P., Dauphas, N., Bollinger, C.,
 Etoubleau, J., Bischoff, A., and Yamaguchi, A. 2016.
 Evidence from Tm Anomalies for Non-CI Refractory
 Lithophile Element Proportions in Terrestrial Planets
 and Achondrites. Geochimica et Cosmochimica Acta 176:
 1–17.
- Barrat, J.-A., Zanda, B., Moynier, F., Bollinger, C., Liorzou, C., and Bayron, G. 2012. Geochemistry of CI Chondrites: Major and Trace Elements, and Cu and Zn Isotopes. *Geochimica et Cosmochimica Acta* 83: 79–92.
- Bartoschewitz, R., Appel, P., Barrat, J.-A., Bischoff, A., Caffee, M. W., Franchi, I. A., Gabelica, Z., et al. 2017. The Braunschweig Meteorite—A Recent L6 Chondrite Fall in Germany 77: 207–224.
- Bemmerer, D., Boeltzig, A., Grieger, M., Gudat, K., Hensel, T., Masha, E., Osswald, M., et al. 2025. The Felsenkeller Shallow-Underground Laboratory for Nuclear Astrophysics. *European Physical Journal A* 61: 19.
- Bhandari, N., Murty, S. V. S., Shukla, P. N., Shukla, A. D.,
 Mahajan, R. R., Sarin, M. M., Srinivasan, G., et al. 2002.
 Itawa Bhopji (L3-5) Chondrite Regolith Breccia: Fall,
 Classification and Cosmogenic Records. Meteoritics and
 Planetary Science 37: 549–563.
- Bischoff, A. 1985. Al-reiche und intermediäre Chondren in dem H4Chondriten Ybbsitz. *Annalen des Naturhistorischen Museums Wien* 87: 21–31.
- Bischoff, A., Alexander, C. M. O'D., Barrat, J.-A., Burkhardt, C., Busemann, H., Degering, D., Di Rocco, T., et al. 2021. The Old, Unique C1 Chondrite Flensburg—Insight into the First Processes of Aqueous Alteration, Brecciation, and the Diversity of Water-Bearing Parent Bodies and Lithologies. *Geochimica et Cosmochimica Acta* 293: 142–186.
- Bischoff, A., Barrat, J.-A., Bauer, K., Burkhardt, C.,
 Busemann, H., Ebert, S., Gonsior, M., et al. 2017. The
 Stubenberg Meteorite—An LL6 Chondrite Fragmental
 Breccia Recovered Soon after Precise Prediction of the
 Strewn Field. Meteoritics & Planetary Science 52: 1683–1703.
- Bischoff, A., Barrat, J.-A., Berndt, J., Borovicka, J., Burkhardt, C., Busemann, H., Hakenmüller, J., et al. 2019. The Renchen L5-6 Chondrite Breccia—The First

19455100, 0, Downloaded from https://onlinelibrary.wiley.com/doi/10.1111/maps/70060 by Helmholtz Zentrum Muenchen Deutsches Forschungszentrum, Wiley Online Library on [14/10/2025]. See the Terms and Conditions (https://onlinelibrary.wiley.com/doi/10.1111/maps/70060 by Helmholtz Zentrum Muenchen Deutsches Forschungszentrum, Wiley Online Library on [14/10/2025]. See the Terms and Conditions (https://onlinelibrary.wiley.com/doi/10.1111/maps/70060 by Helmholtz Zentrum Muenchen Deutsches Forschungszentrum, Wiley Online Library on [14/10/2025]. See the Terms and Conditions (https://onlinelibrary.wiley.com/doi/10.1111/maps/70060 by Helmholtz Zentrum Muenchen Deutsches Forschungszentrum, Wiley Online Library on [14/10/2025]. See the Terms and Conditions (https://onlinelibrary.wiley.com/doi/10.1111/maps/70060 by Helmholtz Zentrum Muenchen Deutsches Forschungszentrum, Wiley Online Library.wiley.com/doi/10.1111/maps/70060 by Helmholtz Zentrum Muenchen Deutsches Forschungszentrum, Wiley Online Library.wiley.com/doi/10.1111/maps/70060 by Helmholtz Zentrum Muenchen Deutsches Forschungszentrum, Wiley Online Library.wiley.com/doi/10.1111/maps/70060 by Helmholtz Zentrum Muenchen Deutsches Forschungszentrum, Wiley Online Library.wiley.com/doi/10.1111/maps/70060 by Helmholtz Zentrum Muenchen Deutsches Forschungszentrum, Wiley Online Library.wiley.com/doi/10.1111/maps/70060 by Helmholtz Zentrum Muenchen Deutsches Forschungszentrum, Wiley Online Library.wiley.com/doi/10.1111/maps/70060 by Helmholtz Zentrum Muenchen Deutsches Forschungszentrum, Wiley Online Library.wiley.com/doi/10.1111/maps/70060 by Helmholtz Zentrum Muenchen Deutsches Forschungszentrum, Wiley Online Library.wiley.com/doi/10.1111/maps/70060 by Helmholtz Zentrum Muenchen Deutsches Forschungszentrum, Wiley Online Library.wiley.com/doi/10.1111/maps/70060 by Helmholtz Zentrum Muenchen Deutsches Forschungszentrum, Wiley Online Library.wiley.com/doi/10.1111/maps/70060 by Helmholtz Zentrum Muenchen Deutsches Forschungszentrum Wiley Online Library.wiley.com/doi/10.1111/map and-conditions) on Wiley Online Library for rules of use; OA articles are governed by the applicable Creative Commons

- Confirmed Meteorite Fall from Baden-Württemberg (Germany). Geochemistry—Chemie der Erde 79: 125525.
- Bischoff, A., Geiger, T., Palme, H., Spettel, B., Schultz, L.,
 Scherer, P., Schlüter, J., and Lkhamsuren, J. 1993.
 Mineralogy, Chemistry, and Noble Gas Contents of Adzhi-Bogdo—An LL3-6 Chondritic Breccia with L-Chondritic and Granitoidal Clasts. *Meteoritics* 28: 570–78.
- Bischoff, A., and Keil, K. 1983a. CaAlrich Chondrules and Inclusions in Ordinary Chondrites. *Nature* 303: 588–592.
- Bischoff, A. and Keil, K. 1983b. Catalog of Alrich Chondrules, Inclusions and Fragments in Ordinary Chondrites (Special Publication No. 22). UNM, Institute of Meteoritics, Albuquerque, 1–33.
- Bischoff, A., and Keil, K. 1984. Al-Rich Objects in Ordinary Chondrites: Related Origin of Carbonaceous and Ordinary Chondrites and their Constituents. *Geochimica et Cosmochimica Acta* 48: 693–709.
- Bischoff, A., Palme, H., and Spettel, B. 1989. Alrich Chondrules from the Ybbsitz H4chondrite: Evidence for Formation by Collision and Splashing. Earth and Planetary Science Letters 93: 170–180.
- Bischoff, A., Patzek, M., Alosius, R. M. L., Barrat, J.-A., Berndt, J., Busemann, H., Degering, D., et al. 2024. The Anomalous Polymict Ordinary Chondrite Breccia of Elmshorn (H3-6)—Late Re-Accretion after Collision between Two Ordinary Chondrite Parent Bodies, Complete Disruption, and Mixing Possibly about 2.8 Gyr Ago. Meteoritics & Planetary Science 59: 2321–56.
- Bischoff, A., Patzek, M., Barrat, J.-A., Berndt, J., Busemann, H., Degering, D., Di Rocco, T., et al. 2024. Cosmic Pears from the Havelland (Germany): Ribbeck, the Twelfth Recorded Aubrite Fall in History. *Meteoritics & Planetary Science* 59: 2660–94.
- Bischoff, A., Patzek, M., Peters, S. T. M., Barrat, J.-A., Di Rocco, T., Pack, A., Ebert, S., Jansen, C. A., and Kmieciak, K. 2022. The Chondrite Breccia of Antonin (L4-5)—A New Meteorite Fall from Poland with a Heterogeneous Distribution of Metal. Meteoritics & Planetary Science 57: 2127–42.
- Bischoff, A., Reitz, M. P., Roszjar, J., Patzek, M., Barrat, J.-A., Berndt, J., Di Rocco, T., Pack, A., and Weber, I. 2025. Kindberg, the 5th Meteorite Fall in Austria: A Weakly Shocked L6 Chondrite Breccia with High-Pressure Phases. *Meteoritics & Planetary Science*. submitted.
- Bischoff, A., Rubin, A. E., Keil, K., and Stöffler, D. 1983. Lithification of Gas-Rich Chondrite Regolith Breccias by Grain Boundary and Localized Shock Melting. *Earth and Planetary Science Letters* 66: 1–10.
- Bischoff, A., Schleiting, M., and Patzek, M. 2019. Shock Stage Distribution of 2280 Ordinary Chondrites—Can Bulk Chondrites with a Shock Stage S6 Exist as Individual Rocks? *Meteoritics & Planetary Science* 54: 2189–2202.
- Bischoff, A., Schleiting, M., Wieler, R., and Patzek, M. 2018.

 Brecciation among 2280 Ordinary Chondrites—
 Constraints on the Evolution of their Parent Bodies.

 Geochimica et Cosmochimica Acta 238: 516–541.
- Bischoff, A., Scott, E. R. D., Metzler, K., and Goodrich, C.
 A. 2006. Nature and Origins of Meteoritic Breccias. In *Meteorites and the Early Solar System II*, edited by D. S.
 Lauretta, and H. Y. McSween, Jr., 679–712. Tucson: Univ. of Arizona.
- Bischoff, A., and Stöffler, D. 1992. Shock Metamorphism as a Fundamental Process in the Evolution of Planetary

- Bodies: Information from Meteorites. *European Journal of Mineralogy* 4: 707–755.
- Brandstätter, F., Kirchner, E., Kracher, A., and Kurat, G. 1985. Der Meteorit von Ybbsitz: Petrologie und Mineralchemie. *Annalen des Naturhistorischen Museums Wien* 87: 11–20.
- Brown, P. G., McCausland, P. J. A., Hildebrand, A. R.,
 Hanton, L. T. J., Eckart, L. M., Busemann, H., Krietsch,
 D., et al. 2023. The Golden Meteorite Fall: Fireball
 Trajectory, Orbit, and Meteorite Characterization.
 Meteoritics & Planetary Science 58: 1773–1807.
- Busemann, H., Baur, H., and Wieler, R. 2000. Primordial Noble Gases in "Phase Q" in Carbonaceous and Ordinary Chondrites Studied by Closed-System Stepped Etching. *Meteoritics & Planetary Science* 35: 949–973.
- Dalcher, N., Caffee, M. W., Nishiizumi, K., Welten, K. C., Vogel, N., Wieler, R., and Leya, I. 2013. Calibration of Cosmogenic Noble Gas Production in Ordinary Chondrites Based on ³⁶Cl-³⁶Ar Ages. Part 1: Refined Produced Rates for Cosmogenic ²¹Ne and ³⁸Ar. *Meteoritics & Planetary Science* 48: 1841–62.
- Dunn, T. L., Cressey, G., McSween, H. Y., Jr., and McCoy,
 T. J. 2010. Analysis of Ordinary Chondrites Using Powder
 X-Ray Diffraction: 1. Modal Mineral Abundances.
 Meteoritics & Planetary Science 45: 123–134.
- Ebert, S., and Bischoff, A. 2016a. Genetic Relationship between Na-Rich Chondrules and Ca,Al-Rich Inclusions?

 —Formation of Na-Rich Chondrules by Melting of Refractory and Volatile Precursors in the Solar Nebula. Geochimica et Cosmochimica Acta 177: 182–204.
- Ebert, S., and Bischoff, A. 2016b. The Stubenberg (Bavaria) Ordinary Chondrite Breccia: The Latest German Meteorite Fall. *Meteoritics & Planetary Science* 51: #6137.
- Gattacceca, J., Bouvier, A., Grossman, J., Metzler, K., and Uehara, M. 2019. The Meteoritical Bulletin, No. 106. *Meteoritics & Planetary Science* 54: 469–471.
- Gattacceca, J., McCubbin, F. M., Grossman, J., Bouvier, A., Chabot, N. L., D'Orazio, M., Goodrich, C., et al. 2022. The Meteoritical Bulletin, No. 110. *Meteoritics & Planetary Science* 57: 2102–5.
- Graf, T., and Marti, K. 1994. Collisional Records in LL-Chondrites. *Meteoritics* 2: 643–48.
- Gritsevich, M., Moilanen, J., Visuri, J., Meier, M. M. M., Maden, C., Oberst, J., Heinlein, D., et al. 2024. The Fireball of November 24, 1970, as the most Probable Source of the Ischgl Meteorite. *Meteoritics & Planetary Science* 59: 1658–91.
- Haack, H., Sørensen, A. N., Bischoff, A., Patzek, M., Barrat,
 J.-A., Midtskoge, S., Stempel, E., et al. 2019. Ejby—A
 New H5/6 Ordinary Chondrite Fall in Copenhagen,
 Denmark. Meteoritics & Planetary Science 54: 1853–69.
- Heiken, G., Vaniman, D., and French, B. M. eds. 1991. *The Lunar Sourcebook*. Cambridge: Cambridge University Press.
- Hertkorn, N., Harir, M., and Schmitt-Kopplin, P. 2015. Nontarget Analysis of Murchison Soluble Organic Matter by High-Field NMR Spectroscopy and FTICR Mass Spectrometry. *Magnetic Resonance in Chemistry* 53: 754–768.
- Herwartz, D., Pack, A., Friedrichs, B., and Bischoff, A. 2014. Identification of the Giant Impactor Theia in Lunar Rocks. *Science* 344: 1146–50.
- Herzog, G. F., and Caffee, M. 2014. Cosmic-Ray Exposure Ages of Meteorites. In *Treatise on Geochemistry 2nd Ed.*— Vol. 2 Planets, Asteroids, Comets and the Solar System,

19455100, 0, Downloaded from https://onlinelibrary.wiley.com/doi/10.1111/maps.70060 by Helmbluz Zentrum Muenchen Deutsches Forschungszentrum, Wiley Online Library on [14/10.2025]. See the Terms and Conditions (https://onlinelibrary.wiley. on Wiley Online Library for rules of use; OA articles are governed by the applicable Creative Commons

- edited by A. M. Davies, 419–453. Amsterdam, Netherlands: Elsevier.
- Hiesinger, H., Helbert, J., Alemanno, G., Bauch, K. E.,
 D'Amore, M., Maturilli, A., Morlok, A., et al. 2020.
 Studying the Composition and Mineralogy of the
 Hermean Surface with the Mercury Radiometer and
 Thermal Infrared Spectrometer (MERTIS) for the
 BepiColombo Mission: An Update. Space Science Reviews
 216: 110.
- Jenniskens, P., Rubin, A. E., Yin, Q.-Z., Sears, D. W. G., Sandford, S. A., Zolensky, M. E., Krot, A. N., et al. 2014. Fall, Recovery and Characterization of the Novato L6 Chondrite Breccia. *Meteoritics & Planetary Science* 49: 1388–1425.
- Kieffer, S. W. 1975. From Regolith to Rock by Shock. *The Moon* 13: 301–320.
- Leya, I., Hirtz, J., and David, J.-C. 2021. Galactic Cosmic Rays, Cosmic-Ray Variations, and Cosmogenic Nuclides in Meteorites. *The Astrophysical Journal* 910: 136.
- Leya, I., and Masarik, J. 2009. Cosmogenic Nuclides in Stony Meteorites Revisited. *Meteoritics & Planetary Science* 44: 1061–86.
- Lodders, K., and Fegley, B., Jr. 1998. *The Planetary Scientist's Companion*. New York: Oxford University Press. 371.
- Martschini, M., Lachner, J., Hain, K., Kern, M., Marchhart, O., Pitters, J., Priller, A., et al. 2022. 5 Years of Ion-Laser Interaction Mass Spectrometry—Status and Prospects of Isobar Suppression in AMS by Lasers. *Radiocarbon* 64: 555–568.
- Morlok, A., Bischoff, A., Patzek, M., Sohn, M., and Hiesinger, H. 2017. Chelyabinsk—A Rock with Many Different (Stony) Faces: An Infrared Study. *Icarus* 284: 431–442.
- Morlok, A., Renggli, C., Charlier, B., Namur, O., Klemme, S., Reitze, M. P., Weber, I., et al. 2023. A Mid-Infrared Study of Synthetic Glass and Crystal Mixtures Analog to the Geochemical Terranes on Mercury. *Icarus* 396: 115498.
- Namur, O., and Charlier, B. 2017. Silicate Mineralogy at the Surface of Mercury. *Nature Geoscience* 10: 9–13.
- Nier, A. O. 1950. A Redetermination of the Relative Abundances of the Isotopes of Carbon, Nitrogen, Oxygen, Argon and Potassium. *Physical Review* 77: 789–793.
- Niese, S., Köhler, M., and Gleisberg, B. 1998. Low-Level Counting Techniques in the Underground Laboratory "Felsenkeller" in Dresden. *Journal of Radioanalytical and Nuclear Chemistry* 233: 167–172.
- Nishiizumi, K., Regnier, S., and Marti, K. 1980. Cosmic Ray Exposure Ages of Chondrites, Pre-Irradiation and Constancy of Cosmic Ray Flux in the Past. *Earth and Planetary Science Letters* 50: 156–170.
- Norris, T. L., Gancarz, A. J., Rokop, D. J., and Thomas, K. W. 1983. Half-Life of ²⁶Al. *Proceedings, 14th Lunar and Planetary Science Conference, Journal of Geophysical Research Suppl* 8: B331–B333.
- Pack, A., and Herwartz, D. 2014. The Triple Oxygen Isotope Composition of the Earth Mantle and Understanding Δ¹⁷O Variations in Terrestrial Rocks and Minerals. *Earth* and Planetary Science Letters 390: 138–145.
- Pack, A., Höweling, A., Hezel, D. C., Stefanak, M., Beck, A. K., Peters, S. T. M., Sengupta, S., Herwartz, D., and Folco, L. 2017. Tracing the Oxygen Isotope Composition of the Upper Earth Atmosphere Using Cosmic Spherules. *Nature Communications* 8: 15702.

- Pack, A., Tanaka, R., Hering, M., Sengupta, S., Peters, S., and Nakamura, E. 2016. The Oxygen Isotope Composition of San Carlos Olivine on VSMOW2-SLAP2 Scale. Rapid Communications in Mass Spectrometry 30: 1495–1504.
- Palme, H., Spettel, B., and Wänke, H. 1985. Die chemische Zusammensetzung des Meteoriten von Ybbsitz. Annalen des Naturhistorischen Museums Wien 87: 47–51.
- Peters, S. T. M., Alibabaie, N., Pack, A., McKibbin, S. J., Raeisi, D., Nayebi, N., Torab, F., Ireland, T., and Lehmann, B. 2020. Triple Oxygen Isotope Variations in Magnetite from Iron-Oxide Deposits, Central Iran, Record Magmatic Fluid Interaction with Evaporite and Carbonate Host Rocks. Geology 48: 211–15.
- Popova, O., Jenniskens, P., Emel'Yanenko, V., Kartashova, A., Biryukov, E., Khaibrakhmanov, S., Shuvalov, V., et al. 2013. Chelyabinsk Airburst, Damage Assessment, Meteorite Recovery and Characterization. *Science* 342: 1069–73.
- Reitze, M. P., Weber, I., Morlok, A., Hiesinger, H., Bauch, K. E., Stojic, A. N., and Helbert, J. 2021a. Mid-Infrared Spectroscopy of Crystalline Plagioclase Feldspar Samples with Various Al,Si Order and Implications for Remote Sensing of Mercury and Other Terrestrial Solar System Objects. Earth and Planetary Science Letters 554: 116697.
- Reitze, M. P., Weber, I., Morlok, A., Hiesinger, H., Bauch, K. E., Stojic, A. N., and Helbert, J. 2021b. Mid-Infrared Spectroscopy of Anorthosite Samples from near Manicouagan Crater, Canada, as Analogue for Remote Sensing of Mercury and Other Terrestrial Solar System Objects. *Journal of Geophysical Research: Planets* 126: e2021JE006832.
- Riebe, M. E. I., Welten, K. C., Meier, M. M. M., Wieler, R.,
 Barth, M. I. F., Ward, D., Laubenstein, M., et al. 2017.
 Cosmic-Ray Exposure Ages of Six Chondritic Almahata
 Sitta Fragments. *Meteoritics & Planetary Science* 52: 2353–74.
- Rochette, P., Sagnotti, L., Bourot-Denise, M., Consolmagno,
 G., Folco, L., Gattacceca, J., Osete, M. L., and Pesonen,
 L. 2003. Magnetic Classification of Stony Meteorites: 1.
 Ordinary Chondrites. *Meteoritics & Planetary Science* 38: 251–58
- Rout, S. S., Keil, K., and Bischoff, A. 2010. Bulk Chemical Compositions of Al-Rich Objects from Rumuruti (R) Chondrites: Implications for their Origin 70: 35–53.
- Rubin, A. E. 2003. Chromite-Plagioclase Assemblages as a New Shock Indicator; Implications for the Shock and Thermal Histories of Ordinary Chondrites. *Geochimica et Cosmochimica Acta* 67: 2695–2709.
- Ruf, A., Kanawati, B., Hertkorn, N., Yin, Q. Z., Moritz, F., Harir, M., Lucio, M., et al. 2017. Previously Unknown Class of Metalorganic Compounds Revealed in Meteorites. Proceedings of the National Academy of Sciences 114: 2819–24.
- Rüfenacht, M., Morino, P., Lai, Y.-J., Fehr, M. A., Haba, M. K., and Schönbächler, M. 2023. Genetic Relationships of Solar System Bodies Based on their Nucleosynthetic Ti Isotope Compositions and Sub-Structures of the Solar Protoplanetary Disk. Geochimica et Cosmochimica Acta 355: 110–125.
- Salisbury, J. W., D'Aria, D. M., and Jarosewich, E. 1991. Midinfrared (2.5-13.5 μm) Reflectance Spectra of Powdered Stony Meteorites. *Icarus* 92: 280–297.

19455100, 0, Downloaded from https://onlinelibrary.wiley.com/doi/10.1111/maps.70060 by Helmholtz Zentrum Muenchen Deutsches Forschungszentrum, Wiley Online Library on [14/10/2025]. See the Terms and Conditions (https://onlinelibrary.wiley.com/terms and-conditions) on Wiley Online Library for rules of use; OA articles are governed by the applicable Creative Commons

- Schmitt-Kopplin, P., Gabelica, Z., Gougeon, R. D., Fekete, A., Kanawati, B., Harir, M., Gebefuegi, I., Eckel, G., and Hertkorn, N. 2010. High Molecular Diversity of Extraterrestrial Organic Matter in Murchison Meteorite Revealed 40 Years after its Fall. *Proceedings of the National Academy of Sciences* 107: 2763–68.
- Schmitt-Kopplin, P., Harir, M., Kanawati, B., Tziotis, D., Hertkorn, N., and Gabelica, Z. 2012. Chemical Footprint of the Solvent Soluble Extraterrestrial Organic Matter Occluded in Soltmany Ordinary Chondrite. *Meteorite Journal*, Special issue *Soltmany* 1–2: 79–92.
- Shrbeny, L., Krzesinska, A. M., Borovicka, J., Spurný, P., Tyminski, Z., and Kmieciak, K. 2022. Analysis of the Daylight Fireball of July 15, 2021, Leading to Meteorite Fall and Find near Antonin, Poland, and a Description of the Recovered Meteorite. *Meteoritics & Planetary Science* 57: 2108–26.
- Spurný, P. 2016. Instrumentally Documented Meteorite Falls:
 Two Recent Cases and Statistics From All Falls. In Asteroids: New Observations, New Models. Proceedings IAU Symposium 318, edited by S. Chesley, A. Morbidelli, R. Jedicke, and D. Farnocchia, 69–79. Cambridge: Cambridge University Press.
- Spurný, P., and Borovička, J. 2025. Orbits of Meteorites Recovered Thanks to the European Fireball Network in the Last Decade (abstract #5212). Meteoritics & Planetary Science 60; 87th Annual Meeting of the Meteoritical Society 2025 (LPI Contrib. No. 3088).
- Spurný, P., Borovička, J., Baumgarten, G., Haack, H., Heinlein, D., and Sørensen, A. N. 2017. Atmospheric Trajectory and Heliocentric Orbit of the Ejby Meteorite Fall in Denmark on February 6, 2016. Planetary and Space Science 143: 192–98.
- Spurný, P., Borovicka, J., Haloda, J., Shrbeny, L., and Heinlein, D. 2016. Two Very Precisely Instrumentally Documented Meteorite Falls: Žďár Nad Sázavou and Stubenberg—Prediction and Reality (abstract #6221). *Meteoritics & Planetary Science* 51: A591, Special Issue.
- Steiger, R. H., and Jäger, E. 1977. Subcommission on Geochronology: Convention on the Use of Decay Constants in Geo- and Cosmochronology. Earth and Planetary Science Letters 36: 359–362.
- Stöffler, D., Hamann, C., and Metzler, K. 2018. Shock Metamorphism of Planetary Silicate Rocks and Sediments: Proposal for an Updated Classification System. *Meteoritics & Planetary Science* 53: 5–49.
- Stöffler, D., Keil, D., and Scott, E. R. D. 1991. Shock Metamorphism of Ordinary Chondrites. Geochimica et Cosmochimica Acta 55: 3845–67.
- Taylor, L. A., Pieters, C. M., Keller, L. P., Morris, R. V., and McKay, D. S. 2001. Lunar Mare Soils Space Weatheirng and the Major Effects of Surface-Correlate Nanophase Fe.

SUPPORTING INFORMATION

Additional supporting information may be found in the online version of this article.

Table S1: Details about the recovered pieces of Haag. **Figure S1:** Images of the second recovered Haag piece H02.

- Journal of Geophysical Research-Atmospheres 106: 27985–
- The Meteoritical Bulletin Database. 2025. https://www.lpi.usra.edu/meteor/metbull.cfm
- Tziotis, D., Hertkorn, N., and Schmitt-Kopplin, P. 2011.

 Kendrick-Analogous Network Visualisation of Ion
 Cyclotron Resonance Fourier Transform (FTICR) Mass
 Spectra: Improved Options to Assign Elemental
 Compositions and to Classify Organic Molecular
 Complexity. European Journal of Mass Spectrometry 17:
 415–421.
- Váci, Z., Agee, C. B., Humayun, M., Ziegler, K., Asmerom, Y., Polyak, V., Busemann, H., et al. 2020. Unique Achondrite Northwest Africa 11042: Exploring the Melting and Breakup of the L Chondrite Parent Body. *Meteoritics & Planetary Science* 55: 622–648.
- Vernazza, P., Delbo, M., King, P. L., Izawa, M. R. M., Olofsson, J., Lamy, P., Cipriani, F., et al. 2012. High Surface Porosity as the Origin of Emissivity Features in Asteroid Spectra. *Icarus* 221: 1162–72.
- Ward, D., Bischoff, A., Roszjar, J., Berndt, J., and Whitehouse, M. J. 2017. Trace Element Inventory of Meteoritic Ca-Phosphates. American Mineralogist 102: 1856–80.
- Weber, I., Morlok, A., Grund, T., Bauch, K. E., Hiesinger, H., Stojic, A., Grumpe, A., et al. 2018. A Mid-Infrared Reflectance Database in Preparation for Space Missions. *Lunar and Planetary Science Conference* 48: #1430.
- Weber, I., Reitze, M. P., Heeger, M., Adolphs, T., Morlok, A., Stojic, A. N., Hiesinger, H., Arlinghaus, H. F., and Helbert, J. 2021. The Effect of Excimer Laser Irradiation on Mid-IR Spectra of Mineral Mixtures for Remote Sensing. Earth and Planetary Science Letters 569: 117072.
- Weber, I., Reitze, M. P., Morlok, A., Stojic, A. N., Hiesinger, H., Schmedemann, N., Bauch, K. E., Pasckert, J. H., and Helbert, J. 2023. Mid-IR Spectral Properties of Different Surfaces of Silicate Mixtures Before and After Excimer Laser Irradiation. *Icarus* 404: 115683.
- Weyrauch, M., Horstmann, M., and Bischoff, A. 2018. Chemical Variations of Sulfides and Metal in Enstatite Chondrites—Introduction of a New Classification Scheme. *Meteoritics & Planetary Science* 53: 394–415.
- Wieler, R. 2002. Cosmic-Ray-Produced Noble Gases in Meteorites. Reviews in Mineralogy and Geochemistry 47: 125–170.
- Williams, N. H., Fehr, M. A., Parkinson, I. J., Mandl, M. B., and Schönbächler, M. 2021. Titanium Isotope Fractionation in Solar System Materials. *Chemical Geology* 568: 120009.
- Zipfel, J., Bischoff, A., Schultz, L., Spettel, B., Dreibus, G.,
 Schönbeck, T., and Palme, H. 2010. Mineralogy,
 Chemistry, and Irradiation Record of Neuschwanstein
 (EL6) Chondrite. Meteoritics & Planetary Science 45: 1488–1501.
- **Figure S2:** Computed tomography (CT) slices of the Haag sample H02.
- **Figure S3:** Haag thin section (PL24076) studied in this work.
- **Figure S4:** IR spectrum of the groundmass of the brownish fragment in Figure 4b.

conditions) on Wiley Online Library for rules of use; OA articles are governed by the applicable Creative Commons Licenso

Figure S5: Ti isotope composition of Haag.

Figure S6: Neon three isotope plot.

Figure S7: Argon three isotope plot.

Figure S8: Mass spectrum of the Haag methanolsoluble compounds.

Figure S9: Measured specific ²²Na activity and related shielding depth.

Figure S10: Bern-plot.
Figure S11: ²⁶Al from gamma and instrumental accelerator mass spectrometry.

Figure S12: Compositional space in CHOMg of the Haag meteorite.